Hase, N., **Doktor, D.**, **Rebmann, C.**, Dechant, B., **Mollenhauer, H.**, Cuntz, M. (2022):
Identifying the main drivers of the seasonal decline of near-infrared reflectance of a temperate deciduous forest
Agric. For. Meteorol. **313** , art. 108746

http://dx.doi.org/10.1016/j.agrformet.2021.108746

Identifying the main drivers of the seasonal decline of near-infrared reflectance of a temperate deciduous forest

Niklas Hase[a], Daniel Doktor[a], Corinna Rebmann[a], Benjamin Dechant[b], Hannes Mollenhauer[a] and Matthias Cuntz[c]

[a] *Helmholtz Centre for Environmental Research GmbH – UFZ, Permoserstraße 15, 04318 Leipzig, Germany*

[b] *Department of Landscape Architecture and Rural Systems Engineering, Seoul National University, Seoul, South Korea*

[c] *Université de Lorraine, AgroParisTech, INRAE, UMR Silva, 54000 Nancy, France*

ABSTRACT

The physical mechanisms behind correlations of earth observations and remote sensing products are of vital importance. The so-called 'near-infrared reflectance of vegetation' (NIR_V) and gross primary production (GPP) show high correlations among different ecosystems and temporal scales but the underlying relationship is still poorly understood. NIR_V is defined as the product of normalized difference vegetation index (NDVI) and near-infrared (NIR) canopy reflectance (R^{NIR}). We examined this relationship in the case of a temperate deciduous forest in Germany. GPP, R^{NIR} and NIR_V all exhibited a strong rise during leaf development in spring and a continual decline after the maximum in early summer. The decline of NIR_V in late summer was mainly driven by the decline of R^{NIR}, since NDVI remained saturated.

Here we tested the attributions of the decline of R^{NIR} to changes in leaf area index, leaf optical properties, canopy structure, sun-sensor geometry, or understory vegetation by measuring seasonal variations of those factors of the temperate deciduous forest. Leaf area was nearly constant between May and mid September, leaf albedo decreased slightly, leaf angles increased over time towards more vertical leaves, and understory reflectance decreased considerably.

We simulated the seasonal decline of R^{NIR} of the forest using the radiative transfer model FRT and quantified the sensitivity of the decline to variations in the measured parameters. FRT captured well the observed seasonal decline of R^{NIR} by Sentinel 2 using the measured optical and structural properties. Decreasing understory reflectance alone explained 43% of the simulated decrease of R^{NIR}, while leaf angle variations explained 31%, the solar zenith angle (SZA) 21%, leaf albedo 7%, and LAI 0%. The effect size of the SZA depended on the viewing angle and would hence be different for different satellites and for local instruments. The results may help to better understand and help to track seasonal changes in forest structure and leaf optical properties using remote sensing techniques. They also suggest that the proposed link between the seasonal

evolution of GPP and $\mathrm{NIR_V}$ may be weaker than expected.

1. Introduction

The so-called 'near-infrared reflectance of vegetation' ($\mathrm{NIR_V}$) was defined by Badgley et al. (2017) as the product of the normalized difference vegetation index (NDVI) and near-infrared (NIR) canopy reflectance ($\mathrm{R^{NIR}}$)

$$\mathrm{NIR_V} = \mathrm{NDVI} \cdot \mathrm{R^{NIR}} \tag{1}$$

where

$$\mathrm{NDVI} = \frac{\mathrm{R^{NIR}} - \mathrm{R^{red}}}{\mathrm{R^{NIR}} + \mathrm{R^{red}}} \tag{2}$$

and $\mathrm{R^{red}}$ is the red canopy reflectance. Light absorbance of leaves is relatively low in the NIR for dry matter, water and brown pigments are the main absorbing components and high in the red wavebands due to photosynthetic pigments (Feret et al., 2008). This results in high $\mathrm{R^{NIR}}$, low $\mathrm{R^{red}}$, high NDVI, and high $\mathrm{NIR_V}$ for vegetated surfaces. $\mathrm{NIR_V}$ has recently been proposed as a proxy for photosynthesis or plant productivity at ecosystem scale (Badgley et al., 2017; Butterfield et al., 2020). $\mathrm{NIR_V}$ shows higher correlation to gross primary productivity (GPP) on monthly time scales compared to other proxies, namely NDVI, fPAR and the MODIS GPP product (Badgley et al., 2017), especially for deciduous forests (Badgley et al., 2019). On shorter time scales of half hours to days the so-called 'near-infrared radiance of vegetation' ($\mathrm{NIR_{V,rad}}$), which may be defined as the product of $\mathrm{NIR_V}$ and upwelling photosynthetic active radiation, outperformed $\mathrm{NIR_V}$ in predicting GPP for a wide set of functional, structural and weather conditions (Baldocchi et al., 2020), and even outperformed solar-induced fluorescence in case of soy bean and corn (Dechant et al., 2020). Newest developments include, e.g. a nonlinear NDVI generalization (Camps-Valls et al., 2021), which improves the GPP monitoring accuracy.

We hypothesize that $\mathrm{NIR_V}$ correlates well with GPP for deciduous forests due to the $\mathrm{R^{NIR}}$ decline in late summer. This decline is a well-known phenomenon, but the underlying mechanisms are still poorly understood (Reaves et al., 2018) and was observed for broadleaf, coniferous, deciduous, and evergreen forests (Blackburn and Milton, 1995; Jiao et al., 2014; Keenan et al., 2014; Reaves et al., 2018; Butterfield et al., 2020), croplands (Butterfield et al., 2020), and grasslands (Jiao et al., 2014). Other vegetation indices indicated a similar seasonal decline, for example the enhanced vegetation index (EVI) (Zhang et al., 2004; Nagai et al., 2010a,b; Keenan et al., 2014; Yang et al., 2014), green vegeta-

---

ORCID(s):

tion fraction from spectral mixture analysis (Fisher et al., 2006; Reaves et al., 2018) and the green chromatic coordinate (GCC) (Keenan et al., 2014; Yang et al., 2014; Liu et al., 2020).

R^{NIR} change may be related to tree adjustments in order to optimize whole canopy light interception (Niinemets, 2010; Raabe et al., 2015; Badgley et al., 2017). Canopy reflectance is controlled by multiple factors: LAI (overstory and understory), leaf albedo (sum of leaf reflectance and transmittance), leaf angle distribution, clumping of leaves into shoots, branches and crowns, understory reflectance, and bark and branch reflectance (Ross, 1981). These factors exhibit differences in their seasonal variations as well as their effect on R^{NIR}. The seasonal R^{NIR} decline is probably caused by simultaneous changes of several of those factors, possibly also by interactions between the factors. Main drivers of declining R^{NIR} in simulation studies were total LAI (understory + overstory) (Rautiainen et al., 2009; Suviste et al., 2007), understory LAI (Häusler et al., 2016) and the SZA (Suviste et al., 2007).

Generally, variations of both leaf albedo and LAI may have large effects on R^{NIR}. During spring leaves thicken and the growing amount of intercepting and absorbing leaf tissues increases leaf reflectance and decreases leaf transmittance. However, during summer variations of leaf albedo (Demarez, 1999; Mõttus et al., 2014; Hovi et al., 2017; Reaves et al., 2018) and LAI (Wang et al., 2005; Keenan et al., 2014; Croft et al., 2015; Reaves et al., 2018) of temperate deciduous forests are small and their contribution to the change in R^{NIR} should hence be small too. There have been only few observations of a high seasonal decline of NIR leaf albedo, e.g. for white oak (Yang et al., 2016) or shaded oak leaves (Demarez, 1999).

The leaf angle distribution (LAD) of vegetation is an important determinant of spectral canopy reflectance and transmittance, and hence absorption and photosynthesis (Jacquemoud, 1993; Vicari et al., 2019). LADs may vary between species, heights, light regimes, and throughout the growing season. In high light conditions trees may avoid leaf damage from excessive light exposure by orienting leaves more vertically or rolling them (Niinemets, 2010). A vertical orientation of leaves in the top allows light to penetrate deeper into the canopy, increasing light interception in the lower canopy and reducing canopy reflectance. In low light conditions leaves tend to be more regularly dispersed, horizontally oriented, flat, thin, and large in order to maximize light interception (Raabe et al., 2015).

LADs are often assumed to be constant and given by basic distributions (e.g. spherical) while Reaves et al. (2018) highlighted the importance of seasonal LAD changes to the seasonal R^{NIR} decline. They found the highest decline at sites with high vegetation cover and species with high leaf angle variations. Still, seasonal LAD LADs have rarely been measured due to labor intensive retrieval methods (Ryu et al., 2010). Novel automated methods may facilitate LAD measurements in the future using terrestrial LIDAR scanning in case of small canopies (Liu et al., 2019; Vicari et al., 2019) or UAV for higher canopies (McNeil et al., 2016).

The understory (also called background or forest floor) may also be an important driver of R^{NIR} changes, due to its potentially strong seasonal variations and its high effect on canopy reflectance in the near infrared (Eriksson et al., 2006; Pisek et al., 2016; Pisek, 2018; Pisek et al., 2021). The fraction of light transmitted through the canopy (upwards or downwards) is much higher in the NIR than in the visible waveband. In the red spectral region, leaves appear dark (leaf albedo below 0.15), since most light is absorbed by photosynthetic pigments and leaf transmittance is nearly zero. In the NIR spectral region, leaves are semi-opaque and scatter most of the light (leaf albedo 0.85-0.98). Strong seasonal variations of forest understory reflectance were found for hemiboreal forests (Rautiainen et al., 2011; Nikopensius et al., 2015; Pisek et al., 2016), open and dense black spruce forests (Pisek et al., 2016), open Aleppo pine plantations (Pisek et al., 2016) and for open Mediterranean cork oak woodlands (Häusler et al., 2016). Understory development was higher for fertile soils (Pisek et al., 2016) and lower in case of water limitation (Pisek et al., 2016; Häusler et al., 2016). Understory reflectance not only affects NIR_V but also other vegetation indices such as NDVI (Pisek et al., 2016), EVI and LAI products (Eriksson et al., 2006).

The sun and viewing angles may have large effects on R^{NIR} due to the anisotropy of forest canopy reflectance (Ross, 1981; Middleton, 1991; Syren, 1994; Roy et al., 2017; Ma et al., 2019). The sun angle varies diurnally and seasonally. The viewing angle may vary between different instruments and sites from narrow angle sensors in nadir direction to hemispherical sensors. SZA controls the influence of the understory on canopy reflectance, depending on canopy cover and the contrast between the understory and canopy. With decreasing SZA towards summer solstice, the gap fraction in the beam direction increases, more light is intercepted and reflected by the understory (Huete, 1987). Similarly, with decreasing viewing zenith angle (VZA) the gap fraction in the viewing direction increases and the fraction of understory seen by the observer increases (Rautiainen et al., 2008). A surge in canopy reflectance is caused by the hot spot effect, in case the viewing direction and the illumination direction coincide (Hapke et al., 1996).

The SZA dependency of R^{NIR} varies with respect to the contrast between overstory and understory. For a cotton canopy, for example, this dependency was substantially influenced by the underlying soil (Huete, 1987). Hemispherical R^{NIR} of a spruce-hemlock forest increased slightly with increasing SZA (Deering et al., 1994). Conversely, nadir R^{NIR} of young spruce, pine and hardwood stands decreased with increasing SZA (Kimes et al., 1986; Syren, 1994). Little variation in R^{NIR} was found for SZAs from 31° to 71° for shinnery oak in near-nadir viewing angles due to little contrast between leaves and the sandy soil in these wavelengths (Deering et al., 1992).

The goal of the study presented here was to identify the drivers behind the seasonal R^{NIR} decline of a temperate deciduous forest in Germany. We hypothesised that this decline is caused by seasonal variations of the SZA, LAI, leaf albedo, leaf angles, and understory reflectance. We expected interactions between the SZA and understory reflectance, a low contribution of the understory for a high SZA, and a decreasing influence of the understory with increasing SZA. We tested our hypothesis conducting a seasonal measurement campaign in 2018 combined with radiative transfer simulations using the Forest Reflectance and Transmittance (FRT) model (Kuusk and Nilson, 2000)). The innovation of our approach was to isolate the effects of individual drivers on the seasonal decrease of R^{NIR} using a forest radiative transfer model and measured seasonal changes of the most relevant factors simultaneously as input. Previously mostly isolated factors were considered and measured time series of some of the relevant factors were scarce.

2. Materials and Methods

To identify the drivers of the seasonal decline of NIR canopy reflectance R^{NIR} of the deciduous forest at Hohes Holz, we measured optical and structural variables and quantified their effects on canopy reflectance using the forest radiative transfer model (FRT, (Kuusk and Nilson, 2000)). We parametrised FRT according to our repeated measurements and to inventory data (see below). We complemented the forest observations with frequent measurements at an arboretum because of the difficulty of accessing leaves in the upper canopy layer.

2.1. Field Sites

The measurement campaign was conducted in a deciduous forest at Hohes Holz (Saxony-Anhalt, Germany) as well as the arboretum of Leipzig University. Inventory data on locations, species, heights, and diameters at breast height in the forest were recorded once in 2018 while measurements of optical forest properties (reflectance of leaves and understory) and forest structure (leaf angles, leaf area, gap fraction) were collected repeatedly. The leaf reflectance measurements in the forest were complemented by measurements in the arboretum since due to logistics sunlit leaves could not be sampled for all tree species in the forest. The measurement frequency was every three weeks at the forest and weekly in the arboretum.

The forest Hohes Holz is located in Saxony-Anhalt near the Harz Mountains (52.08 °N, 11.22 °E, 193 m above sea level) in a temperate climate. The measurements were conducted within a fenced area of 1 ha size with a tree density of 260 trees per ha (Holtmann et al. (2021), c.f. Figure 1).

Elevations do not differ more than 10 m in the study area, ensuring robust flux recordings. As the dominant tree species in the fenced area were *F. sylvatica* (beech), *C. betulus* (hornbeam), *Q. robur* (oak), and *B. pendula* (birch), these species were selected for all measurements. While the basal areas of *F. sylvatica*, *C. betulus* and *Q. robur* were similar (10.6 m^2, 12.5 m^2 and 12.5 m^2, respectively), there were very few *B. pendula* trees in the fenced area (basal area 1.2 m^2, c.f. Table 1).

An eddy covariance tower of 50 m height is located within the fenced area, which was used for leaf angle measurements and leaf sampling for leaf reflectance measurements (Figure 2). GPP was derived from NEE (net ecosys-

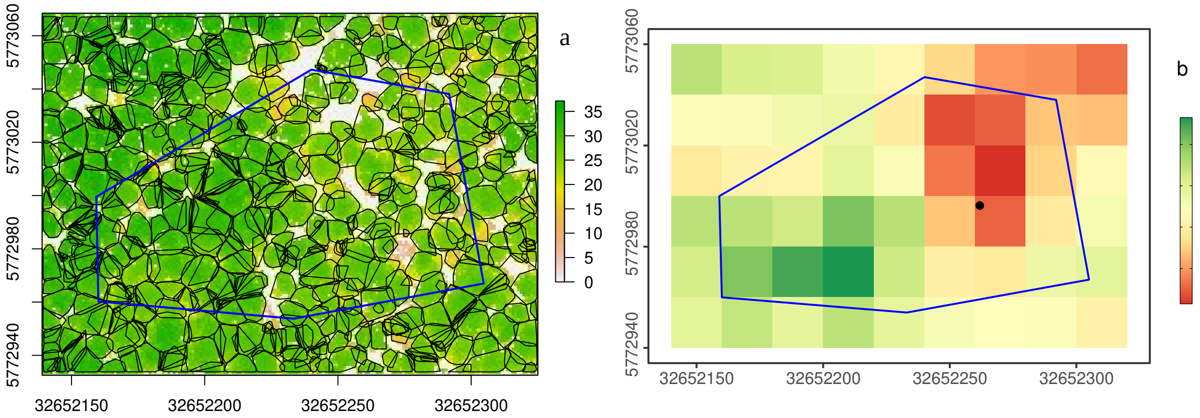

Figure 1: Tree height and NIR reflectance at Hohes Holz: left, tree heights and crown projection shapes at the deciduous forest Hohes Holz. The blue polygon encloses the fenced area. Right, mean canopy NIR reflectance from Sentinel 2, band 8a, from June to Sept 2018. The blue polygon encloses the fenced area and the black circle marks the position of the 50 m-high eddy covariance tower. Coordinates are given in UTM 32.

Table 1
Number of trees (absolute numbers and in percent), mean tree height and basal area (absolute numbers and in percent) of the four dominant tree species at the deciduous forest Hohes Holz within the fenced area of 1 ha.

species	count		mean height	basal area	
	#	%	m	m^2	%
F. sylvatica	94	36	24.0	10.6	29
C. betulus	87	33	17.5	12.5	34
Q. robur	72	28	29.5	12.5	34
B. pendula	7	3	28.0	1.2	3

tem productivity) measured with an eddy covariance system at 49 m tower height consisting of a CSAT-3 ultrasonic anemometer (Campbell Scientific Inc., Logan, UT, USA) and a LI-7500 infrared gas analyser (Li-Cor Inc., Lincoln, NE, USA). High-frequency data (20Hz) were acquired with a Campbell data logger and the Eddymeas data acquisition software (Kolle and Rebmann, 2007). Half-hourly fluxes were processed from high frequency raw data with the EddyPro®software (v. 7.0.6). Flux partitioning of NEE into GPP and ecosystem respiration was subsequently performed according to (Wutzler et al., 2018) with the REddyProc package.

The arboretum is located in Großpösna in Saxony (51.25 °N, 12.48 °E, 150 m above sea level) and is managed by the Leipzig University, Germany. The trees in the arboretum were planted as seedlings in 2012 and are widely spaced with a minimum distance of three meters between trees. Most leaves were exposed to sunlight during the day as the trees were between 1.5 m and 4 m high.

2.2. Observations

2.2.1. Sentinel 2 satellite data

Seasonal near-infrared canopy reflectance measurements were retrieved from Sentinel 2 satellite data (band 8a) at 20 m spatial resolution. We selected a rectangular area of 7×4 Sentinel pixels covering the fenced area ($x_{\text{min}} = 652160$,

Figure 2: The eddy covariance tower and surrounding forest at the study site Hohes Holz. The picture taken by a drone in October 2016 is facing west and shows also forest stands beyond the fenced area.

x_{max} = 652300, y_{min} = 5772960, y_{max} = 5773040, UTM32, Figures 3 and 1). In total 53 Sentinel 2a/b observations from tile T32UPC (radiances) of the year 2018 were downloaded from the 'Copernicus Open Access Hub'. These were converted to bottom of atmosphere reflectances using ESA's processor Sen2Cor (Louis et al., 2016) in a (semi-)automatic processing routine. Sen2Cor produced accurate results in the red and moderate accuracy in the NIR in Atmospheric Correction Inter-Comparison exercise (Doxani et al., 2018). Sen2Cor also produces a so-called scene classification (SCL) image, identifying pixels contaminated by clouds or haze. We used only pixels that were assigned to the classes 'vegetation' (number of pixels n=3410) or 'bare soil' (n=283) in the SCL image and thus identified as cloud-free.

2.2.2. Leaf Albedo

Leaves were sampled at several heights in the forest and in the arboretum at heights between 1 m and 2 m in all four cardinal directions on two to three trees (Table 2). In the forest, leaves were cut either by hand or by using a 6 m tree pruner (Fiskars Germany GmbH, Erlangen). The collected leaves were stored in plastic bags, cooled and reflectance spectra were measured within 2 hours after collecting. In the arboretum leaves were sampled at the tree without cutting them. Leaf reflectance was measured using the Field Spec 4 attached to a plant probe (Analytic Spectral Devices, Boulder, Colorado, USA). White reference measurements were performed by using diffuse reflective synthetic material (ODM98-F03, Gigahertz-Optik GmbH, Türkenfeld, Germany), which was calibrated against a calibrated white reference panel (Spectralon , SphereOptics GmbH, Herrsching, Germany). Reflectance spectra were averaged over five leaves from each sampling point.

Table 2
Sampling heights for leaf albedo at the forest site Hohes Holz and number of sampled trees at the arboretum in Großpösna.

species	Hohes Holz heights [m]	arboretum # of trees
F. sylvatica	2, 17, 24	3
C. betulus	2	2
Q. robur	3, 25, 28	3
B. pendula	13, 24	3

Leaf albedo was calculated as the sum of measured leaf reflectance and simulated leaf transmittance. For each leaf reflectance measurement, the PROSPECT parameters were determined inverting the leaf optical properties model PROSPECT (version 5B, Feret et al. (2008); Jacquemoud and Baret (1990)) and consequently used as input parameters for PROSPECT to simulate leaf transmittance. PROSPECT was inverted following the approach of Dechant et al. (2017) using DEoptim (Mullen et al., 2011), an implementation of the differential evolution algorithm in the R programming language (R Core Team, 2018). The performance of the leaf parameter inversion was evaluated comparing measured and inverted leaf dry matter content and leaf water content at 9 sampling points, where 5 spectra from 5 leaves were collected on June 16th. We measured fresh weight and dry weight of leaves. The leaves were oven dried at 70 °C for 48 hours. Leaf area was measured using a flatbed scanner and the software ImageJ (Schneider et al., 2012).

2.2.3. Understory Reflectance and Greenness

Understory nadir reflectance (ground + vegetation) spectra were measured according to the procedure described by Rautiainen et al. (2011). Along two transects of 50 m length each, an understory spectrum and a white reference spectrum were recorded every 8 m. For the understory spectra the nadir downward-pointing fiber optic of the FieldSpec 4 ASD spectroradiometer was held at the outstretched hand at approximately 1 m height. The sampled area corresponds to a circle with a diameter of about 44 cm. The white reference spectra were recorded by holding the downward-pointing fiber optic 10 cm above the calibrated white Spectralon panel, which was held horizontally. In case of direct sunlight conditions an umbrella was used to shade the panel and the understory within the field of view of the fibre optic.

Understory greenness was quantified via the green chromatic index (gcc, Keenan et al., 2014) from digital photos of the understory taken at 108 points (data not shown here). At each point four photos were taken with a Canon PowerShot D10 digital camera (Canon Inc., Tokyo, Japan) mounted on a rack at 1.5 m height facing the four cardinal directions with an downward facing field of view and an off-nadir view angle of 37.5°.

2.2.4. Leaf Angles

Leaf angle measurements were derived from leveled digital photographs (Ryu et al., 2010) of trees near the tower at heights below 32 m. Leaf angles of leaves whose lamina was aligned perpendicular to the view were measured as the angle between the zenith and the normal (orthogonal) of the leaf surface using the software ImageJ.

2.2.5. Gap Fraction, LAI and Canopy Transmittance

Gap fraction was estimated from digital photography at 104 points according to Piayda et al. (2015). 79 of the 108 points were arranged on a regular grid with 10 m distance between points and 24 points were arranged on 3 finer grids (8 points each) with 5 m distance between points. Photos were taken with a Canon PowerShot D10 digital camera (Canon Inc., Tokyo, Japan) mounted on a rack oriented at 0° zenith angle and at 57.3° zenith angle facing north. Among all zenith angles, digital photography taken at 57.3° zenith angle are least affected by the leaf angle distribution (Wilson, 1960). Gap fraction was calculated as the ratio of gap pixels to the total number of pixels for each photo. The number of gap pixels was estimated using the eCognition software (Trimble Germany GmbH). The camera has a 1/2.3 inch (ca. 6.16×4.62 mm) CCD sensor and a focal length of 6.2 mm enclosing a horizontal and vertical viewing angle span of 53° and 41°, respectively.

Leaf area index (LAI) of the overstory was estimated from hemispherical fisheye photography (EOS 100D, Canon) at 36 sampling points at 1.5 m height above the ground between May and November. The processing of the images and estimation of LAI was performed by ICOS-ETC (Viterbo, Italy).[1] Binarisation of the sky pixels for gap fraction calculation was performed via Ridler et al. (1978). The LAI was inverted from the gap fraction with the ellipsoidal leave angle distribution (Thimonier et al., 2010). Clumping was estimated using Lang and Xiang (1986) with 45° segments. Additionally, litter traps were used to estimate LAI. Leaves were collected 8 times using 25 litter traps (0.5 m^2) distributed in 5 continuous plots (CPs) according to the ICOS standard procedures for Class 1 Ecosystem stations (Gielen et al., 2018). After separation in fractions and species, their dry mass was determined.

Canopy transmittance was measured via a mobile wireless sensor network (Mollenhauer et al., 2017) consisting of nine nodes. One node was mounted at 50 m height on the tower and eight nodes were distributed at the forest floor at 2 m height. The positions of the eight sensors at the forest floor were chosen among the 104 gap fraction measurement points using latin hypercube sampling such that the nadir gap fraction measured at the sensor positions in 2017 corresponded to a representative sample of the gap fraction distribution at all points. The mean gap fraction measured at the position of the 8 nodes via the method described above in 2017 from May 23rd to August 30th was in 0.025, 0.039, 0.040, 0.046, 0.079, 0.084, 0.086, 0.117. The maximum gap fraction of all measurements was 0.698 on 23rd of May and of all considered nodes 0.135 on 1st of August. Each node consisted of two multispectral (4 wavelengths), nadir-oriented sensors: one sensor was looking downward, measuring upwelling radiance, and the one sensor was looking upward, measuring downwelling irradiance. The measurement frequency of sensors was simultaneously every 5 minutes. The center wavelengths of the sensors were 665 nm, 705 nm, 740 nm, and 865 nm. Canopy transmittance was

---

[1] `https://etc-ua.github.io/LeafAreaIndex.jl/LAI.html`

calculated as the mean ratio of irradiance at the forest floor and irradiance at 50 m height between 11 am and 2 pm CET under diffuse sky conditions. Only diffuse sky conditions were selected to exclude the effect of the sunangle. Sky conditions were defined as diffuse for a diffuse to total shortwave downward radiation (SWDR) ratio higher than 0.8. SWDR was measured using a sunshine pyranometer (SPN1, Delta-T Devices Ltd., Cambridge, U.K.)

2.2.6. Auxiliary Measurements

Branch reflectance was measured with an ASD plant probe (Analytic Spectral Devices, Boulder, Colorado, USA) without the leaf-clip for all species at 1 m height. White reference measurements where performed the same way as for leaf albedo. The number of sampled spectra were 6, 5, 6, 8 for *F. sylvatica*, *C. betulus*, *Q. robur*, and *B. pendula*, respectively. Branch reflectance was computed as basal area weighted mean of species mean bark reflectance. Rainfall was measured at 50 m height above the ground using a tipping bucket rain gauge (Adolf Thies GmbH & Co. KG, Göttingen, Germany). Precipitation measurements from 1971-2000 were taken from a DWD (Climate Data Center: Historische tägliche Niederschlagsbeobachtungen für Deutschland, Version v007, 2019) station close by at 52.10 °N, 11.23 °E. Incoming PAR was measured at 50 m height with a Quantum PAR Sensor (LI190R; LI-COR Biogeosciences, Lincoln NE, USA). NIR canopy reflectance at 860 *nm* was measured from the top of the tower with a hyperspectral sensor: QE65000 (Ocean Optics, Dunedin, FL, USA) with 1 min temporal resolution (Lange et al., 2017).

2.3. Simulations

We simulated radiative fluxes within the canopy in the visible and the near-infrared using a radiative transfer model. Modelled NIR reflectance $\mathrm{R}^{\mathrm{NIR}}$ was compared to canopy reflectance observations from Sentinel 2.

2.3.1. Forest Radiative Transfer Model

We used the Forest Reflectance and Transmittance model FRT (Kuusk and Nilson, 2000), which is well suited to interpret multispectral remote sensing data of forest canopies at a wide range of sun and viewing angles (Kuusk et al., 2014). FRT is a one-dimensional radiative transfer model, including tree and crown geometry sub-models. It includes the model of leaf optical properties spectra PROSPECT (Feret et al., 2008), and includes routines for automated estimation of model parameters. FRT distinguishes direct and diffuse radiative fluxes as well as single and multiple scattering. Single scattering is the sum of specular and diffuse scattering using directional gap probabilities from the geometrically modeled trunk and crown shapes. FRT can hence account, for example, for the hot spot effect of the sun. Directional understory reflectance is calculated in FRT with a thin layer approximation (Kuusk, 2001). Good performance of FRT was demonstrated during the RAdiation transfer Model Intercomparison (RAMI) exercises (Widlowski et al., 2015).

Table 3

FRT parameters for the forest Hohes Holz in 2018 retrieved from the measurement campaign and inventory data. Reflectance and albedo values are listed for the 860 nm wavelength. For parameters with seasonal variations, minimum and maximum values are given. See the text for explanations of the parameters.

Parameter	Unit	Value
stand density	trees ha^{-1}	260
tree height	m	23.5
DBH	m	0.32
crown radius	m	3.1
crown form	-	elliptical
leaf eln3[a]	-	4.5-5.3
leaf modal angle	°	8-16
leaf albedo	-	0.94-0.96
leaf area index	m^2 m^{-2}	3.0-5.3
branch area index	m^2 m^{-2}	0.7
branch reflectance	-	0.47
shoot length	m	0.1
shoot shading coefficient	-	0.95
understory reflectance	-	0.40-0.51
tree distribution parameter	-	2.3
crown length	m	4

[a] eln3 $= -\ln(1-\varepsilon)$, where ε is the eccentricity of the leaf angle distribution.

2.3.2. Model Parametrisation

Repeated measurements of optical and structural properties of the forest in 2018 were used for the parametrisation of the model. These translated into a total of 16 parameters (Table 3) where values for tree density, tree height and DBH were taken from forest inventory data. Mean optical and geometrical properties of the different tree species were averaged, weighted by basal area. The crown radius was estimated from DBH for each tree species following Bohn et al. (2014, , suppl. Eq. (3)). Crown form was set elliptical.

The leaf angle distribution was parametrised with the elliptical leaf angle distribution in FRT [Eq. (A1) in Kuusk (1995)]. The elliptical distribution has two parameters, eccentricity and leaf modal angle, and was fitted to the tree density weighted leaf angle distributions of the measured leaf angles of the four species. Leaf albedo was given as direct input to FRT (not PROSPECT parameters), calculated as weighted mean by basal area. Mean leaf albedo did not include measurements from sunlit leaves of *C. betulus*, because those trees were smaller than the other species at Hohes Holz so that sunlit leaves were mainly from *F. sylvatica* and *Q. robur*. Overstory leaf area index (LAI) was measured repeatedly (Section 2.2.5).

Branch area of trees was estimated assuming cylinders with mean tree height and DBH. Branch reflectance was calculated as the area weighted mean. Branch reflectance for individual tree species was 0.476, 0.480, 0.466, and 0.503 for *F. sylvatica*, *C. betulus*, *Q. robur*, and *B. pendula*, respectively. Shoot length was set to 0.1 m and shoot shading coefficient to 0.95.

Nadir reflectance observations of the understory (ground and vegetation) were fed into the two-layer radiative transfer sub-model of FRT for simulating the directional understory reflectance.

The wavelength dependent fraction of direct to total incoming radiation is calculated inside FRT via the radiative transfer model 6S (Vermote et al., 1997). At minimum solar zenith angle in June and July the fraction of direct to total incoming radiation is 0.90, 0.87 on September 19th and 0.82 on October 25th.

In the last step, the tree distribution parameter and the crown length parameter were estimated simultaneously from gap fraction measurements. The radiative transfer within forests is affected by the tree distribution and crown lengths which alter the directional gap fraction. Gap fraction increases with increasing clumping and with decreasing crown length, where the effect of crown length is larger at high viewing zenith angles. The tree distribution parameter describes whether trees are distributed regularly ($c_j < 1$), random ($c_j = 1$) or clumped ($c_j > 1$). We minimised the absolute value of the difference between measured and simulated gap fraction at 0° and 57.3° viewing angle. The tree distribution parameter, c_j, was estimated as 2.3 and the crown length was estimated as 4 m. Simulated and measured gap fractions were 0.16 and 0.14 at 0° viewing angle and 0.07 and 0.07 at 57.3°, respectively. To compare gap fraction estimates from digital photography and simulated directional gap fraction, simulated gap fraction was integrated over the field of view of the digital camera.

The effects of measurement uncertainties on FRT simulation outcomes was quantified for leaf albedo, understory reflectance and LAI by repeating FRT simulations after adding or subtracting the standard deviation to the mean of the measurements. This analysis was not performed for leaf angles, since the leaf angles parameters were derived from the distribution of leaf angles, not only from the mean.

2.3.3. Simulation Runs

The literature review identified five variables ($v_1, ..., v_5$) as potentially important for the development of NIR canopy reflectance: leaf albedo, understory reflectance, leaf angle, SZA, and LAI. Factorial model experiments were designed following the idea of first-order and total-order Sobol' sensitivity indexes (Saltelli et al., 2008). The experiments were implemented by conducting three types of simulation runs, which we termed *all constant except* v_i, v_i *constant*, and *default*.

For the *all constant except* v_i runs all variables except v_i were kept constant using the respective measurement of Aug 18th, while v_i was changed according to observations in 2018. For *all constant except leaf angle* all variables were kept constant except the two leaf angle variables *eln3* and the *leaf modal angle* variable. For the v_i *constant* runs the v_i was set constant using the respective measurement of Aug 18th but all other variables changed over time according to the observations. If a specific variable was set constant, e.g. leaf albedo, the simulation run was appropriately called *leaf albedo constant*. These runs were compared to the *default* run, where all variables changed with time (according to observations). We defined the direct effect ($\delta_{\mathrm{d,i}}$ for $i = 1, \dots, 5$) as:

$$\delta_{\mathrm{d,i}} = \frac{R^{\mathrm{NIR}}_{\text{all constant except } v_i}(\text{Sept } 19^{\text{th}}) - R^{\mathrm{NIR}}_{\text{all constant except } v_i}(\text{May } 23^{\text{rd}})}{R^{\mathrm{NIR}}_{\text{default}}(\text{Sept } 19^{\text{th}}) - R^{\mathrm{NIR}}_{\text{default}}(\text{May } 23^{\text{rd}})} \tag{3}$$

where $R^{\mathrm{NIR}}_{\textit{all constant except } v_i}(t)$ and $R^{\mathrm{NIR}}_{\textit{default}}(t)$ are the NIR canopy reflectance at date t for the *all constant except* v_i and *default* simulation runs, respectively. The *all constant except* v_i runs measured hence the direct effect ($\delta_{\mathrm{d,i}}$) of variable v_i on the NIR reflectance output. The *default* runs included the effects of all variables and showed the highest NIR reflectance change over time.

All other variables but the variable v_i varied in the runs named v_i *constant*, which includes interactions and correlations between the varying variables. The total effect ($\delta_{\mathrm{t,i}}$ for $i = 1, \dots, 5$) including interactions and correlations between variables can hence be calculates as:

$$\delta_{\mathrm{t,i}} = 1 - \frac{R^{\mathrm{NIR}}_{v_i \text{ constant}}(\text{Sept } 19^{\text{th}}) - R^{\mathrm{NIR}}_{v_i \text{ constant}}(\text{May } 23^{\text{rd}})}{R^{\mathrm{NIR}}_{\text{default}}(\text{Sept } 19^{\text{th}}) - R^{\mathrm{NIR}}_{\text{default}}(\text{May } 23^{\text{rd}})} \tag{4}$$

where $R^{\mathrm{NIR}}_{v_i\, \textit{constant}}(t)$ is the NIR canopy reflectance at date t for the v_i *constant* simulation runs.

This resulted in eleven simulations: one *default* simulation with all variables changing, and two simulations per target variable v_i (v_i *constant* and *all constant except* v_i, $i = 1, \dots, 5$).

2.3.4. Further simulations

We assessed the validity of our understory measurements at Hohes Holz by also simulating $\mathrm{R}^{\mathrm{NIR}}$ replacing our measurements in the simulations with the understory measurements from on open cork oak woodland of Häusler et al. (2016). We compared the effect of the two time series of seasonal understory reflectance using the FRT model.

We quantified the interaction between understory reflectance, solar zenith angle and viewing zenith angle by calculating the contribution of understory to simulated $\mathrm{R}^{\mathrm{NIR}}$ (i.e. the fraction of upwelling radiation above the canopy that was scattered by the understory). The contribution of understory to $\mathrm{R}^{\mathrm{NIR}}$ (α_{s}) was calculated for different viewing zenith angles (θ_v) and solar zenith angles (θ_s) as

$$\alpha_{\mathrm{s}} := \frac{R^{\mathrm{NIR}}(\theta_s, \theta_v, \rho_s) - R^{\mathrm{NIR}}(\theta_s, \theta_v, \rho_s = 0)}{R^{\mathrm{NIR}}(\theta_s, \theta_v, \rho_s)}, \tag{5}$$

where understory reflectance (ρ_{s}) was either set to the measured value from August 16th or to 0.

We analyzed the effect of the viewing zenith angle on the seasonal decline of NIR canopy reflectance. Seasonal trajectories of FRT simulated R^{NIR} were compared for different viewing zenith angles and for hemispherical field of view for the measured optical and structural parameters.

We analyzed the effect of LAI on the seasonal decline of R^{NIR} by comparing simulated seasonal trajectories of R^{NIR} for constant LAI values (LAI= 0, 1, ..., 5), while all other parameters varied according to the measured values.

3. Results

3.1. GPP and R^{NIR} at Hohes Holz

The correlation between GPP and NIR_V at Hohes Holz was higher ($R^2 = 0.65$) than between GPP and NDVI ($R^2 = 0.4$) due to the seasonal decline of R^{NIR}. Satellite seasonal R^{NIR} devolution is almost identical with local canopy R^{NIR}: R^2=0.95 between Juni-November (on respective cubic spline smoothings). GPP, R^{NIR} and NIR_V all exhibited a strong rise during leaf development in spring and a continual decline after the maximum in early summer while the NDVI remained constant until senescence (Figure 3). It is hence very likely that the decline of NIR_V in late summer was mainly driven by the decline of R^{NIR}. The NDVI remained constant since a) the seasonal changes of red canopy reflectance (R^{red}) were small compared to the absolute values of R^{NIR} (c.f. eq. (2)) and b) the seasonal changes of R^{NIR} had little effect on NDVI since R^{NIR} is much larger than R^{red}.

3.2. Leaf Albedo

Differences of leaf albedo between the four cardinal directions were small for all species and dates at the arboretum. The seasonal mean of the difference between maximum and minimum NIR leaf reflectance of the four different directions over all measurement dates was below 0.017 for all species (standard error of the mean (SEM) ≤ 0.02). We consequently only show and analyse the mean values per species and measurement date. The performance of the inversion procedure for estimating the PROSPECT leaf parameters from measured leaf reflectance spectra was good, as we found a high correlation between measured and inverted leaf dry matter content ($R^2 = 0.96$, RMSE = 0.0023, n=9) and leaf water content ($R^2 = 0.98$, RMSE = 0.0017, n=9).

Leaf reflectance measurements increased during the season for all species with the highest values for *B. pendula* (≈0.46-0.49) and lowest for *C. betulus* (≈0.43-0.46) (Figure 4). Only *F. sylvatica* exhibited a slightly decreasing leaf reflectance within the top measurements. We found elevated leaf reflectances with increasing measurement height within the canopy, most notably for *F. sylvatica* (+0.07). Leaf reflectance was similar between the arboretum and sunlit top measurements at the forest, except for oak, where derived transmittance values were very low for the forest. Again, measurements of the four different directions at the arboretum were similar for all species and therefore averaged.

Leaf transmittance simulations decreased during the season for most species and heights, except for middle and top

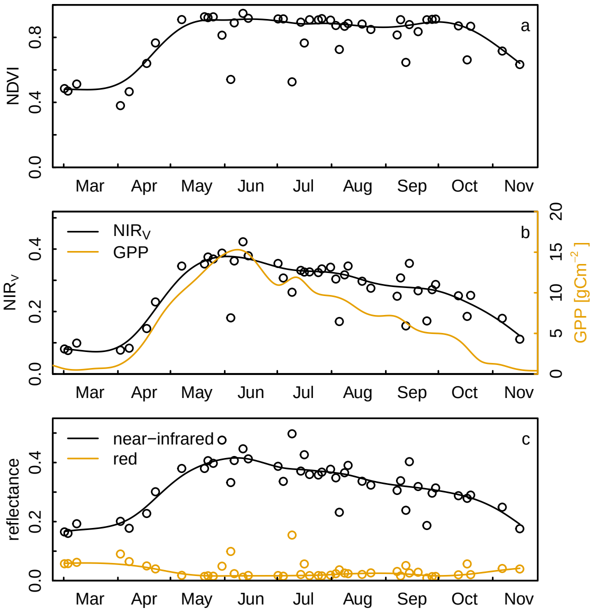

Figure 3: Satellite canopy reflectance products from Sentinel 2 at the deciduous forest at Hohes Holz, Germany in 2018: a) normalized difference vegetation index NDVI, b) NIR_V and gross primary productivity (GPP), and c) near-infrared reflectance (R^{NIR}, center wavelength = 865 nm, bandwidth = 33 nm) and red reflectance (center wavelength = 664 nm, bandwidth = 38 nm). Lines are smoothed using a cubic spline.

measurements of *F. sylvatica* which showed no clear trend or increased, respectively. Absolute values of leaf transmittance differed ranging from ≈0.57 for *C. betulus* to ≈0.4 for *Q. robur* (bottom). We found lowered leaf transmittance with increasing measurement height within the canopy, most notably for *Q. robur*. Leaf transmittance was similar between the arboretum and top simulations in the forest for *F. sylvatica* and *B. pendula*, while values for *Q. robur* where much lower in the top of the forest than in the arboretum.

Leaf reflectance measurements are more coherent than leaf transmittance simulations between arboretum and Hohes Holz and also between top and bottom measurements in the latter. The resulting seasonal variations of leaf albedo (sum of leaf reflectance and leaf transmittance) were small for most species and heights at both study sites. Leaf albedo values largely correspond to leaf transmittance simulations regarding the seasonal evolution, differences between top/bottom canopy measurements, and also regarding species specific differences. Absolute values and seasonal evolution of leaf albedo differed mostly between different heights in the forest and between the forest site and the arboretum. Leaf albedo increased with canopy depth, since leaf transmittance increased more than leaf reflectance decreased. For *B. pendula* in the arboretum and in the top measurement at the forest, mean leaf albedo remained constant throughout the measurement period (May 23rd to Sept 19th) at around 0.94. For the other species leaf albedo slightly decreased at the arboretum, most notably for *C. betulus* (down to ≈0.91). Leaf albedo at the forest site Hohes Holz showed a slightly different picture. At species level, only *B. pendula* exhibited similar magnitudes across both heights,

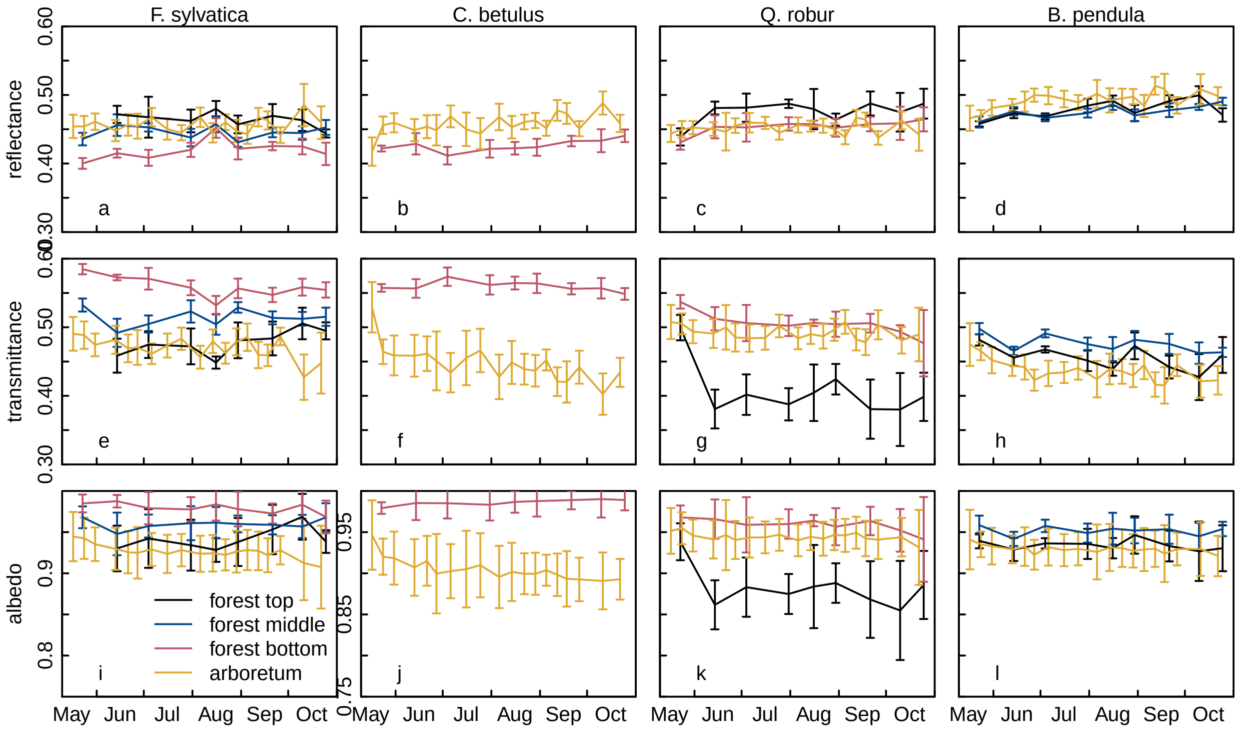

Figure 4: Seasonal variations of leaf reflectance (a-d), leaf transmittance (e-h) and leaf albedo (i-l), which is the sum of leaf reflectance and transmittance, at the forest site Hohes Holz and the arboretum in Großpösna in 2018. In the forest, leaf reflectances were measured at different heights in the canopy with sunlit leaves at the top (≥ 24 m) of the canopy and completely shaded leaves at the bottom (< 16 m) of the canopy (c.f. Table 2). The error bars denote the standard deviation (SD) for reflectance and transmittance, and the square root of the squared sum of SD of reflectance and SD of transmittance for albedo.

comparable to the respective mean arboretum values. Most other species showed substantially higher albedo at the bottom (*C. betulus*, ≈0.98) and even at the top (*F. sylvatica*) with the exception of *Q. robur* where albedo decreased down to below 0.9.

3.3. Understory Reflectance

Mean understory NIR reflectance (860 nm) decreased almost linearly from 0.52 in April down to 0.43 in September 2018 (Figure 5b). We observed the highest measurement variance of all months in June. From September onwards reflectance values exhibited an increase to up to 0.47. This mean seasonal evolution and magnitude is largely reflected in the example transect given in Figure (5a).

Understory reflectance in the Hohes Holz is - dependent on the measurement position along the transects and plant phenology - a mixture of soil and/or vegetation reflectance. Consequently, reflectance values vary considerably within a transect, between the visible and NIR part of the electromagnetic spectrum, and also over the measurement period (Figure 5a). At the beginning of the measurement period (April 2018) the soil was relatively dry and understory

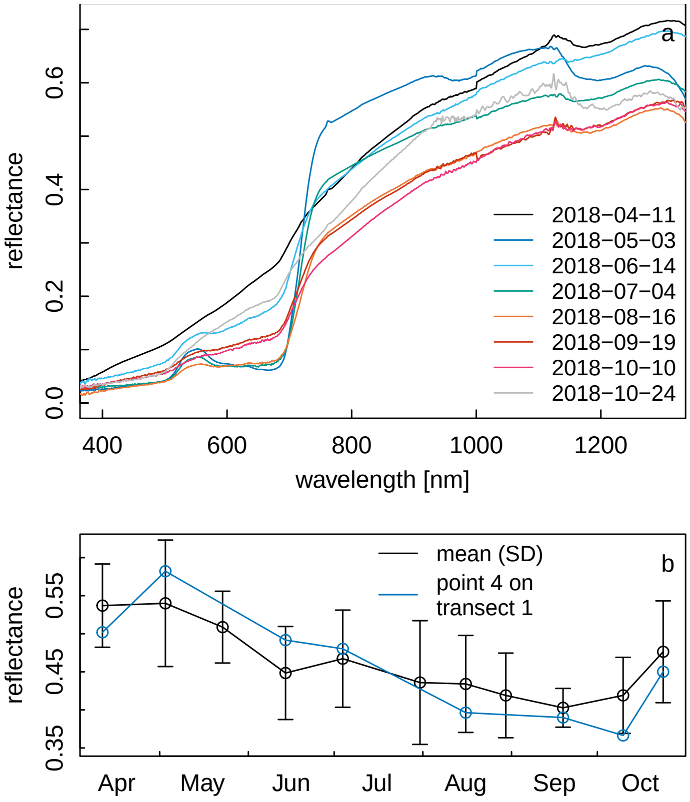

Figure 5: Spectral reflectance of the understory. Top a) Spectral understory reflectance at point 4 of the transect 1 in the forest Hohes Holz at different times of the year. Bottom b) Seasonal development of understory reflectance at 860 nm at point 4 of transect 1 and the mean reflectance of all sampling points on both transects (N = 14, error bars denote the standard deviation).

vegetation had not started to develop. Consequently, the reflectance spectrum resembled a monotone increasing line from the visible into the NIR part. With the development of the understory in May the spectrum exhibited clear vegetation characteristics: a local maximum at around 500 nm (chlorophyll absorption is low between 500 nm and 600 nm) and a steep increase at around 700 nm (the so-called *red edge*) with a plateau thereafter. Towards the end the vegetation period soil characteristics started to dominate again. Yet at slightly lower overall reflectance value (ca. -0.1) was observed due to increased soil moisture after a number of precipitation events.

3.4. Leaf Angles

Figure 6 shows leaf angle distributions (LADs) for the four species at different heights at Hohes Holz in June and August 2018. 0° leaf angle means planophile, horizontal leaves, and 90° leaf angle means erectophile, vertical leaves (Raabe et al., 2015). Leaves with a distribution around 45° are called plagiophile.

In the bottom layer (below 16 m height) all species had more horizontal leaves compared to the middle or top (above 24 m height) layers of the canopy. *F. sylvatica*, *Q. robur* and *B. pendula* all exhibited modal values below 30° at the bottom of the canopy with rather peaked distributions. Leaf angle distributions flattened in the top layer of the

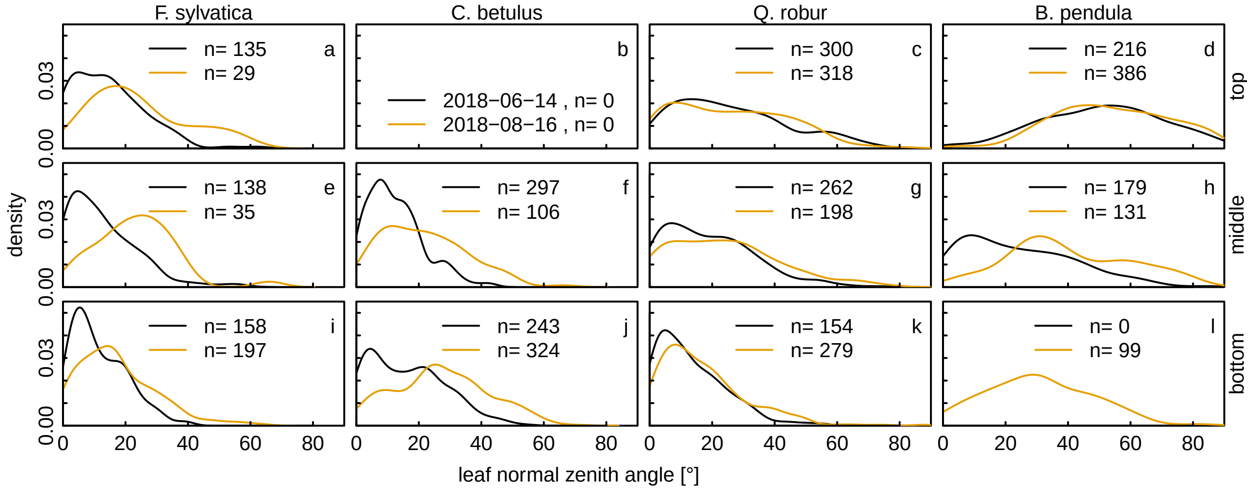

Figure 6: Distributions of leaf normal zenith angles and number of leaf angle measurements (n) for the *F. sylvatica* (a, e, i), *C. betulus* (b,f,j), *Q. robur* (c, g, k) and *B. pendula* (d, h, l) in the top (≥ 24 m, a-d), middle (e-h) and bottom (< 16 m, i-l) layers in the forest Hohes Holz on June 14th (black) and Aug 16th (orange) in 2018.

Table 4
Whole canopy mean and standard deviation (SD) of leaf zenith angle measured distribution in degree. References: [1] Pisek et al. (2013), [2] Raabe et al. (2015), [3] Liu et al. (2019).

species	date	mean	SD	site
F. sylvatica	June 14th	12.9	10.4	Hohes Holz
F. sylvatica	Aug 16th	21.6	13.4	Hohes Holz
F. sylvatica[3]	Jul 17th-Aug 9th	39.7		Bavaria
C. betulus	June 14th	14.4	10.5	Hohes Holz
C. betulus	Aug 16th	25.3	15.9	Hohes Holz
Q. robur	June 14th	19.5	14.4	Hohes Holz
Q. robur	Aug 16th	22.6	16.4	Hohes Holz
Q. robur[1]	Oct 11th	35.8	19.4	garden, Sweden
Q. rubra[2]	June 14th	21.7	13.5	Harvard Forest
Q. rubra[2]	Aug 11th	22.7	14.0	Harvard Forest
B. pendula	June 14th	37.5	18.7	Hohes Holz
B. pendula	Aug 16th	41.6	18.3	Hohes Holz

canopy, which means that more leaves were oriented vertical instead of horizontal.

Between June 14th and August 16th for all species whole canopy mean leaf zenith angle increased (Table 4) and LAD changed towards more plagiophile distributions. At all heights modal values increased slightly and distributions flattened for all species. The changes towards more vertical leaves were little higher for *C. betulus* than for *B. pendula* and *F. sylvatica* and lowest for *Q. robur* and little higher in the middle compared to the bottom and top layers.

3.5. Gap Fraction, LAI and Canopy Transmittance

The variations in canopy structure and transmittance were highest in spring and autumn and small in-between. From April to May, gap fraction dropped from 0.60 to 0.14 (Figure 7) with the onset of leaf unfolding. Between June and mid September, LAI, canopy transmittance and gap fraction remained nearly constant at values around 5.5, 0.22

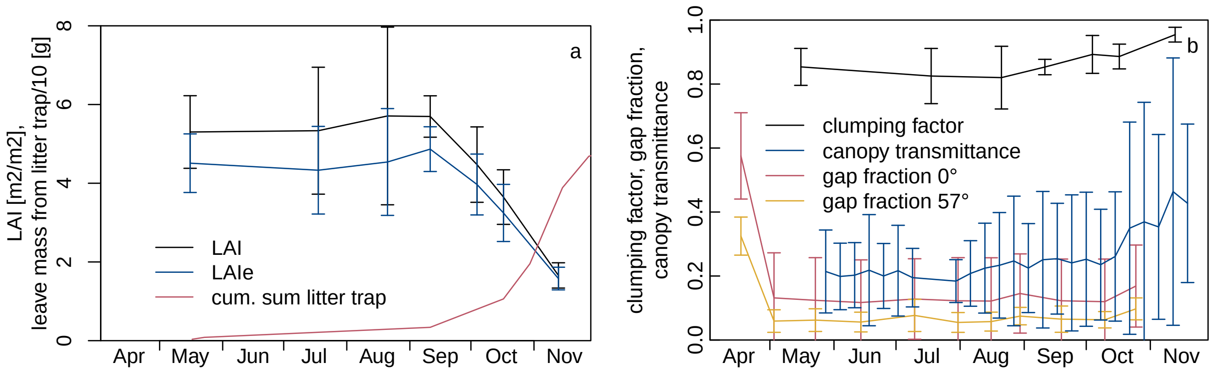

Figure 7: Seasonal variations of the mean (error bars denote the standard deviation at the respective date) of measured variables of canopy structure: overstory leaf area index (LAI), effective overstory leaf area index (LAIe) from hemispherical fisheye photography and cumulative leaf mass from litter trap measurements (a), gap fraction from digital photography with 0° zenith angle (solid line) and 57° zenith angle (dashed line), and near-infrared canopy transmittance (b).

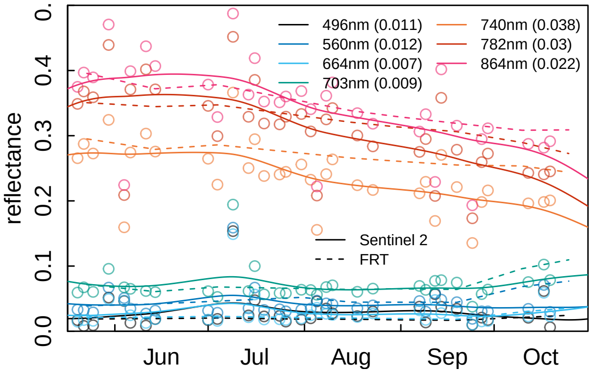

Figure 8: Sentinel 2 band 1-8a canopy reflectance in the fenced area at Hohes Holz in 2018 (circles: values, solid line: smoothing spline) and corresponding simulated canopy reflectance with the FRT model (dashed lines) for the respective wavelengths of the central bands.

and 0.14, respectively. Between mid September and beginning of October overstory LAI started to drop simultaneously with the onset of increased leaf littering. About half a month to a month later, canopy transmittance and gap fraction simultaneously started to increase in the second half of October as a consequence of leaf fall of the dominant tree species.

3.6. Simulated Driving Factors of NIR Canopy Reflectance Changes

Simulated canopy reflectance are well in line with Sentinel 2 canopy reflectance in all visible and NIR bands (Figure 8), especially for the NIR band at 864 nm: $R^2 > 0.9$ for the NIR, but lower for the VIS due to the missing seasonality. Mean absolute differences are less than 1 % for both VIS and NIR. Simulated diffuse canopy transmittance was about 0.1 higher than measured canopy transmittance.

We simulated the development of NIR canopy reflectance R^{NIR} at the forest Hohes Holz from mid May to the end of October with the forest radiative transfer model FRT.

Leaf optical properties changed little in our observations (Figure 4) and leaf albedo also had little effect on simulated R^{NIR} (total effect $\delta_{t,1} = 0.07$, Figure 9a, b). Leaf angle distributions were measured twice at Hohes Holz in 2018 (Figure 6). We took the first observations on 14th June 2018 up to end of July and the second observations on 16th August 2018 from August on to parameterise FRT (Figure 9d). This resulted in a step change of R^{NIR} of 0.02 in the simulations (Figure 9c, run *all constant except leaf angle*). Simulated R^{NIR} was hence too low by this amount at the beginning of the season if the leaf angles measured in August were set constant for the whole season (Figure 9c, run *leaf angle constant* vs. *default*). The total effect of leaf angle $\delta_{t,2} = 0.31$ was the second highest of all total effects.

Understory reflectance changed by 25% from May to September (Figure 9f). This had the largest effect on R^{NIR} (total effect $\delta_{t,3} = 0.43$). Especially R^{NIR} levelling off in October comes mainly from the change of understory reflectance (Figure 9e, run *understory reflectance constant* vs. *default*).

The solar zenith angle (SZA) decreased slightly from 31.5° on May 23rd to 29.0° on June 16th and increased to 50.7° on September 19th and 64.2°on October 25th for our study area (Figure 9h). The change in SZA angle adds 0.02 to the simulated decline of R^{NIR} with a total effect of $\delta_{t,4} = 0.21$ (Figure 9g, run *solar angle constant* vs. *default*).

LAI decreased by about 0.5 between May and September 19th (Figure 9j) and had the smallest total effect among the five considered variables ($\delta_{t,5} = -0.01$, Figure 9i, dotted line).

Accordingly the combined effect of the seasonal changes of leaf albedo, leaf angle, understory reflectance, solar zenith angle, and LAI explains the observed seasonal decline of NIR canopy reflectance R^{NIR}.

4. Discussion

4.1. Limitations

Limitations of the given data set and analysis are discussed below.

The model validation showed high agreements between seasonal Sentinel 2 and simulated visible and NIR canopy reflectance (Figure 8), while discrepancies between simulated and measured diffuse canopy transmittance of ca. 0.1 remained. Canopy transmittance is mainly driven by albedo and effective area of leaf and woody material and gap fraction. The highest uncertainty for those parameters in our analysis remains for woody area and reflectance. Bark reflectance was only measured at heights below 2 m. Simulations with respective values from the literature decreased canopy transmittance slightly, decreased R^{NIR} far below Sentinel 2 values and had little effects on direct and total effects. We conclude, that the general relationship between canopy NIR reflectance and the driving factors is described by the model although simulated and measured fluxes don’t agree fully.

Due to limitation in available measurement equipment, we estimated leaf transmittance from the hyperspectral reflectance measurements by adapting the parameters of the model of leaf optical properties PROSPECT (Feret et al.,

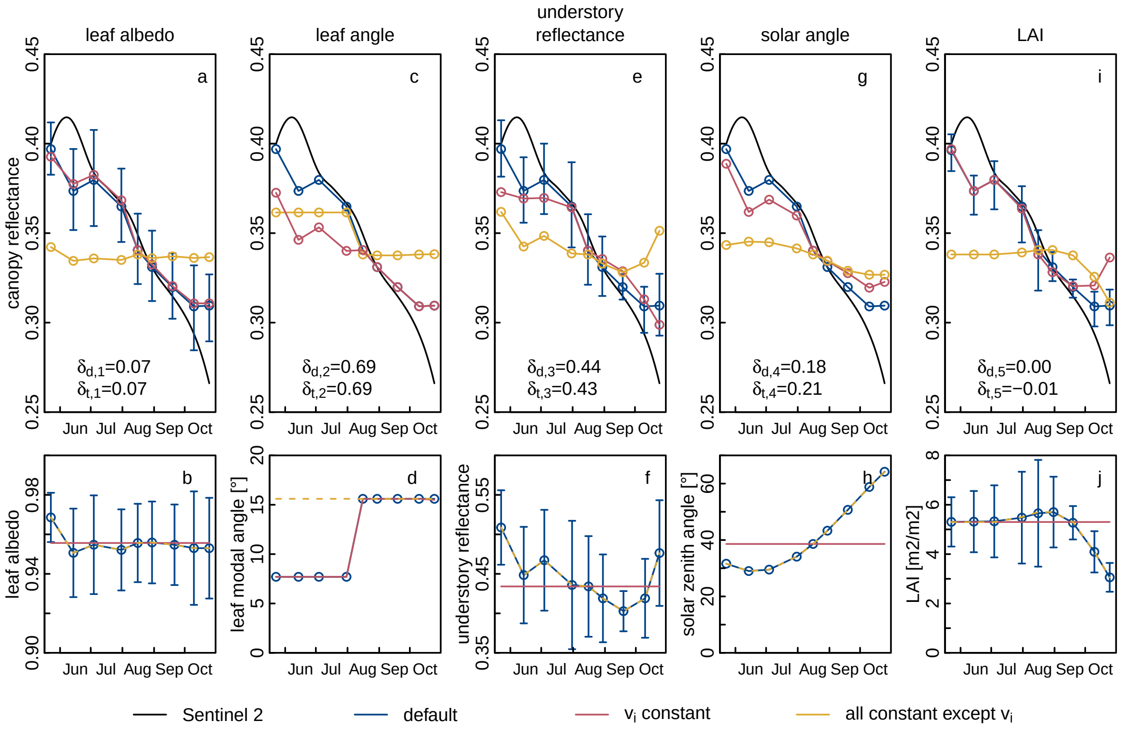

Figure 9: Direct ($\delta_{\mathrm{d,i}}$, Eq. (3)) and total ($\delta_{\mathrm{t,i}}$, Eq. (4)) effects of single variables on the seasonal development of NIR canopy reflectance R^{NIR} at the forest Hohes Holz using the FRT model. The first column (a, b) shows the effect of leaf albedo on canopy reflectance, the second column (c, d) the effect of leaf angle, the third column (e, f) the effect of understory reflectance, the fourth column (g, h) the effect of the solar angle, and the fifth column (i, j) shows the effect of overstory LAI on NIR canopy reflectance R^{NIR}. The upper row (a, c, e, g, i) shows NIR canopy reflectance, the direct effect, and the total effect. The lower row (b, d, f, h, j) shows the input values for the specific variable of the corresponding column in the v_i *constant* run and in the other runs (*default*, *all constant except* v_i). The error bars in the lower row (b, d, f, h, j) show the standard deviation (SD) of the respective variable. The error bars in the upper row (a, c, e, g, i) show the FRT outcome for the same input as the normal run, except the given variable is reduced or increased by its SD, respectively.

2008). We believe that using an integrating sphere would not have changed the results of our study, since a small bias in the absolute value of leaf transmittance would not alter the overall outcome of our analysis, with respect to the effect of the individual parameters on the seasonal decline of R^{NIR}.

Even if the study site is relatively small, it can be regarded as somewhat representative of deciduous forest in Europe with respect to species composition, age, and management. The study area of 1 ha size covers about 25 Sentinel 2 20 m pixels, which we think is enough to provide meaningful and robust results. However, more studies like ours at other sites are needed to check our results.

We investigated drivers of the change in near-infrared (NIR) seasonal canopy reflectance R^{NIR} of a temperate deciduous forest (Hohes Holz) by repeatedly measuring optical and structural properties to parameterise the Forest Reflectance and Transmittance model FRT. We discuss in the following the main drivers of R^{NIR}, their seasonal changes and their contributions to changes in R^{NIR}.

4.2. Understory Reflectance

The few existing studies on the effect of understory reflectance on canopy reflectance support our findings, which state that changing understory reflectance contributed most ($\delta_{t,3} = 43\%$, Figure 9) to the simulated decline of NIR canopy reflectance R^{NIR}. Understory NIR reflectance and respective seasonal changes have rarely been studied (Rautiainen et al., 2011; Pisek et al., 2016; Pisek, 2018). Measurement of understory reflectance is hindered by multiple issues, e.g. by highly variable irradiance under the top canopy, weak signal in some parts of the spectrum and high spatial variability of understory composition (Pisek et al., 2016). Pisek et al. (2016) could estimate understory reflectance for open canopies from multiangular Moderate Resolution Imaging Spectroradiometer (MODIS) bidirectional reflectance distribution function data. For dense forest, where understory LAI is usually lower (Majasalmi and Rautiainen, 2020), the signal of the understory is much attenuated. Rautiainen et al. (2009) simulated seasonal variations of understory reflectance of a birch site, where the decline was similar to our measurements at Hohes Holz for a fertile soil, and much lower and with little variations for an infertile soil. Eriksson et al. (2006) found strong effects (up to 10%) of variable understory LAI on near-infrared canopy reflectance R^{NIR} for sparse stands, also using the FRT model. The effects were lower (2.2% on average) for dense stands (overstory LAI ≥ 3). At one of their sites estimates of LAI and the effect of understory on R^{NIR} where similar to our results. A more detailed comparison of both results would require understory vegetation spectra from Eriksson et al. (2006) or understory LAI estimates for our results.

Häusler et al. (2016) also found a close link between the seasonal evolution (decline) of understory and canopy reflectance in an open cork oak woodland in Portugal. They observed a monotone decrease of understory reflectance with lower absolute values (0.34 on July 25th and 0.29 on Oct 3rd). The herbaceous understory was substantially stressed due to water limitation within this period. This was most likely also the case at Hohes Holz as the summer 2018 was among the driest and hottest on record. Mean monthly precipitation above the canopy in 2018 (mean 1971-2000) was 13 mm (50 mm) in May, 18 mm (69 mm) in June, 23 mm (53 mm) in July, 9 mm (55 mm) in August and 24 mm (42 mm) in September.

Simulated canopy reflectance at Hohes Holz with the understory reflectance measurements from Häusler et al. (2016), instead of our understory reflectance measurements at Hohes Holz, was on average 0.03 lower and decreased by 0.07 from 0.36 on May 23rd to 0.28 on Sept 19th. Our data outperformed those of Häusler at explaining the observed decline in R^{NIR} by Sentinel 2. This engenders confidence in our observations and reaffirms the large impact of the understory on canopy reflectance.

We found substantial spatio-temporal variations of understory reflectances, especially in early summer (Figure 5). On the contrary Jiao et al. (2014) found little variation in understory reflectance between May and September of deciduous forests retrieved from multiangular satellite data. But here, understory (background) reflectance was purely derived from theoretical assumptions (linear combination of proportional reflectances) and not from *in situ* measurements and also on a global scale. The lowest magnitudes at Hohes Holz were observed in the middle of September (0.40), slightly higher than dry litter reflectances of deciduous tree leaves at 860 nm (0.35, wet 0.30) measured by Nagler et al. (2000). We hence concluded that in mid September the understory was mainly composed of senescent leaves and litter.

The spatio-temporal variations of understory reflectance may be caused by multiple factors. The understory surface heterogeneity is high and small positional shifts of the sampled area between different dates cannot be avoided. Also, the relatively low solar zenith angle (SZA) around summer solstice supports frequent changes of sunlit and shaded areas, whereas at higher SZAs, diffuse light conditions dominate, resulting in more homogeneous measurements. However, the seasonal variations may be induced by progressive water limitations throughout the hot and dry summer resulting in leaf area decrease or a comparably early end of vegetation activity. Understory rooting depth is usually limited to the upper soil and therefore prone to prolonged dry weather periods.

The contribution of understory to NIR canopy reflectance R^{NIR} (α_s, eq. (5)) decreased slightly with increasing SZA in our simulations (Figure 10). The decrease of α_s with increasing SZA was weakest for the nadir viewing direction, where the increase of the SZA from 32° to 51° between May 23rd and Sept 19th caused a small decrease from 32% to 30%. For viewing zenith angles of 20°and 40° α_s decreased also slightly with increasing SZA. The fractional vegetation cover was 0.84 (=1-gap fraction in nadir direction). Only for high viewing zenith angles (e.g. 60°) the contribution of understory to R^{NIR} was slightly lower and its decrease with increasing SZA little higher. Accordingly we rejected the hypotheses that the contribution of the understory to R^{NIR} is much lower for high than for low SZAs and that the influence of changing understory reflectance on R^{NIR} should decrease with increasing SZA. On the contrary, the high contribution of the understory to R^{NIR} can be explained by the low leaf absorption in the NIR (below 10%).

The fraction of single scattering by the understory, i.e. the fraction of incoming direct light reflected by the understory without any interaction with the canopy, was low (below 1%) already at low SZAs and converged to 0 with increasing solar zenith angle in our simulations. This may be caused by low gap fractions or the isotropic character of direct light, scattered by the understory. For forest stands with higher gap fractions this fraction of single scattered light from understory may be much higher and thus cause a higher interaction between SZA and understory reflectance (c.f. Section 4.6).

4.3. Leaf Angles

Our simulations indicated that seasonal changes of leaf angles have the second highest contribution ($\delta_{t,2} = 31\%$) among the five tested variables to the seasonal decline of NIR canopy reflectance R^{NIR}. This is despite the fact that the observed changes towards more vertical leaves during the growing season seemed relatively small. Leaf angle dis-

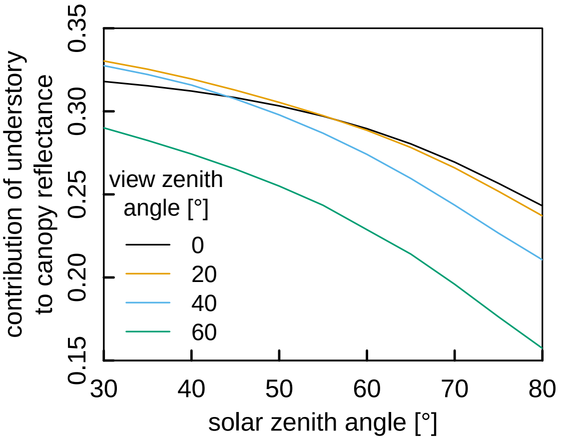

Figure 10: The contribution of the understory to NIR canopy reflectance R^{NIR} (α_s, eq. (5)) simulated with the FRT model for different solar and viewing zenith angles in the antisolar azimuthal direction.

tributions are important determinants of radiative transfer in vegetation canopies since they determine the gap fraction via the leaf area projection on a plane perpendicular to the view direction (also known as G-function Ross (1981)). The contribution of variable leaf specular reflectance to variations of R^{NIR} due to changes in LAD or SZA should be negligible. In the NIR most light is scattered diffusely at the leaf interior and the contribution to leaf reflectance of light reflected specularly at the leaf surface is only significant in the chlorophyll absorption regions and only for high leaf normal illumination angles (Grant, 1987; Bousquet et al., 2005).

The effect of leaf angles on R^{NIR} was still high for LAI=2 but lower for LAI=1 in our simulations. This can be seen in Figure 11c where the slope between July 31rd and August 16th is mainly caused by changes in leaf angles (c.f. Figure 9c). The LAI=0 case in Figure 11c shows again the high effect of all non-overstory-leaf variables on the seasonal decline of R^{NIR}.

The steepening of leaves during summer might be driven by several drivers. For low SZAs more vertical leaves in the top layers increase total canopy absorption, since light penetrates deeper into the canopy due to a decrease in effective leaf area illuminated by the sun (Jacquemoud, 1993). At high SZAs, prevalent at Hohes Holz in late summer, vertical leaves can inrcease whole canopy light interception, e.g. for eucalyptus trees at high latitudes in Australia (King, 1997). The changes of leaf angles towards more vertical leaves in late summer may thus indirect be caused by an increase of the solar zenith angle. This would suggest that the seasonal change in the solar zenith angle has direct and indirect (via leaf angles) effects on canopy NIR reflectance R^{NIR}. The variations of leaf angles may also be caused by increases in lamina mass and area and lengthening or weakening of the petiole with increasing leaf age (Raabe et al., 2015).

Leaf zenith angle measurements of *Q. robur* from Pisek et al. (2013) in a botanical garden in Sweden on Oct

11th was higher compared to our measurements on Aug 16th (Table 4). The tree in Sweden might have more vertical oriented leaves due to potentially higher exposure of light. Park grown individuals of *B. pendula* had e.g. more vertical oriented leaves, especially at lower heights, compared to individuals in closed canopies (Raabe et al., 2015). The LAD of *Q. robur* at Hohes Holz might be more similar to the LAD of *Q. rubra* at Harvard forest, due to more similar forest structures. The steepening of leaves was higher for *Q. robur* at Hohes Holz than for *Q. rubra* at Harvard Forest (Table 4).

In a Bavarian national park mean leaf zenith angles of *F. sylvatica* measured via terrestrial LiDAR scanning (Liu et al., 2019) were about 17° higher compared to Hohes Holz (Table 4). At Hohes Holz LAD in the upper canopy was mostly planophile compared to a rather uniform LAD (all leaf angles) in the upper canopy in Bavaria. LAD at Hohes Holz, however, had much smaller tails, which means fewer leaves with high leaf angles, most probably originating from a higher leaf area index at Hohes Holz than in Bavaria (Cailleret et al., 2014). The differences may be negligible or stem from the different measurement techniques with the LiDAR allowing a larger sample size and hence a better statistic but with less precision per individual leaf compared to the method explained in section 2.2.4.

Observed seasonal variations of leaf inclination in the literature also tend to be largest in spring and early summer and small during the rest of the growing season (e.g. Pisek et al., 2013; Reaves et al., 2018). At Hohes Holz seasonal differences in leaf angle changes could not be identified as the leaf angle distributions were determined only twice.

4.4. Solar and Viewing Angle

Forest canopy reflectance is highly anisotropic and seasonal variations of the sun angle and the viewing angle can have large effects on the measured NIR reflectance. Accordingly, our simulations demonstrated a substantial effect of the solar zenith angle (SZA) — total effect $\delta_{t,4} = 0.21$ — on the seasonal decline of R^{NIR} for the nadir viewing direction (Figure 9g).

However, simulated R^{NIR} was strongly linked to changing viewing zenith angle (VZA, Figure 11a). Different VZA would result in different trajectories of seasonal declining R^{NIR}. For small VZA ($<40°$), simulated R^{NIR} decreased with increasing solar zenith angle for most viewing azimuth angles. For high viewing zenith angle ($> 60°$) simulated R^{NIR} increased with increasing SZA for all view azimuth angles.

In our simulations the hot spot effect and forward scattering caused large differences between the seasonal course of canopy NIR reflectance for low and high VZA. The hot spot is a surge in surface brightness in the back scatter direction (if the directions of the observer and the sun coincide, Figure 11b).

For scatterers which are large compared to the wavelength of incident light, the hot spot is caused by shadow-hiding (Hapke et al., 1996). For low VZA the angle between observer and sun are small in summer at Hohes Holz (Figure 9h) and increases during the season, which causes a decrease of the hot spot effect, i.e. a decrease in R^{NIR} (Figure 11a).

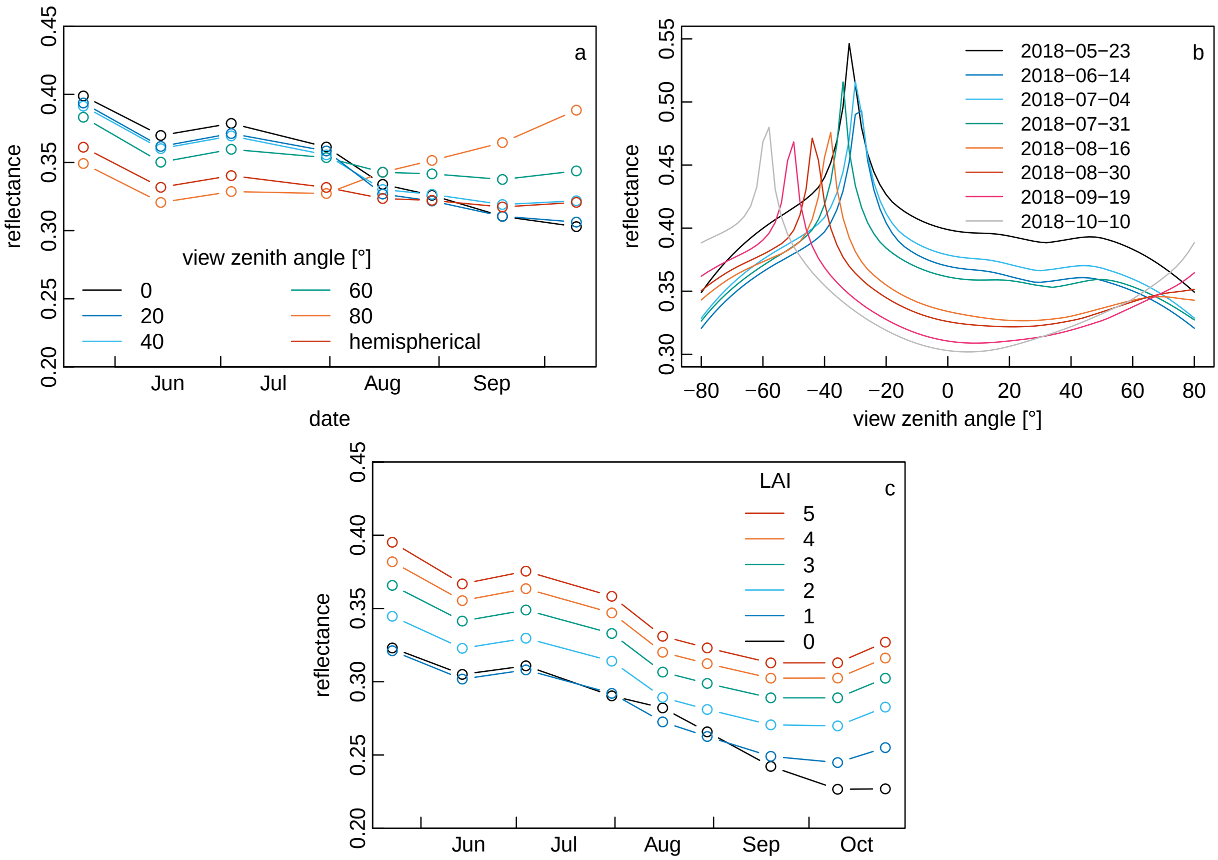

Figure 11: Simulated seasonal NIR canopy reflectance decline at Hohes Holz for (a) different viewing zenith angles (forward scattering in the antisolar direction), (b) bidirectional canopy reflectance in the principal plane, and (c) for constant overstory LAI values at 0° viewing zenith angle.

For high VZA forward scattering is high for high SZA (Figure 11b), which causes an increase R^{NIR} in late summer. The hot spot effect might be even underestimated by FRT due to underestimated backward scattering by FRT (Kuusk et al., 2014).

We also found an increase in R^{NIR} with increasing SZA in the tower based R^{NIR} measurements from the multispectral sensor. For clear sky conditions, minimum NIR reflectance R^{NIR} values were recorded around solar noon (data not shown), but such high viewing zenith angles (> 60°) are extremely rare for any kind of sensor systems, except for hemispherical view setting (e.g. applied by Baldocchi et al. (2020)). For hemispherical view, which has contributions from all view zenith and azimuth angles, simulated R^{NIR} was lower then for nadir viewing direction and the decrease was also lower (Figure 11a). Viewing zenith angles from most satellite observations are between 0-15° (e.g. MODIS Terra/Aqua, Landsat, Sentinel-2 A/B). Still, Roy et al. (2017) found a mean absolute reflectance difference between Sentinel-2A forward and backward scattering of NIR surface reflectance of 0.078 in January, where the maximum observed view zenith angle was 11.93°. Therefore, this effect can most likely be neglected when using data from the above mentioned satellite missions.

4.5. Leaf Albedo

Average NIR leaf albedo of the forest Hohes Holz changed only marginally between May and September 2018 (Figures 4i-l and 9b) and had little effect on the simulated NIR canopy reflectance R^{NIR} ($\delta_{t,1} = 7\%$, Figure 9a). Until late summer leaf reflectance at Hohes Holz remained either constant or increased slightly. At Fontainebleau leaf reflectance increased until June or July and decreased slightly afterwards (Demarez, 1999). The earlier decrease at Fontainebleau might be explained by a later onset of leaf senescence at Hohes Holz or a relative higher sampling of brown leaves. Leaf reflectance of *Q. robur*, *F. sylvatica*, and *C. betulus* at Hohes Holz were similar to measurements at Fontainebleau, while leaf transmittance was about 0.08 to 0.10 lower at Fontainebleau.

To understand why only leaf transmittance differed between Hohes Holz and Fontainebleau we compared leaf mass per area (LMA) measurements at both sites. As mentioned above, NIR leaf transmittance is strongly influenced by leaf thickness (PROSPECT's N parameter) and hence LMA. LMA measurements between June and August were similar for Hohes Holz and Fontainebleau (Demarez, 1999) for most species and heights (for *C. betulus* bottom, *Q. Robur* bottom, *F. sylvatica* bottom and top) except for *Q. robur* top, where LMA was slightly higher at Hohes Holz (105 $\mathrm{gm^{-2}}$) than in Fontainebleau (92 $\mathrm{gm^{-2}}$). Our leaf reflectances were measured with the Field Spec 4 attached to a plant probe and used to estimate leaf transmittance via PROSPECT. Demarez (1999) measured leaf reflectance and transmittance directly in the lab. They then also used PROSPECT to determine leaf traits such as chlorophyll content from the transmittance spectra, and noted very good accordance with independent measurements of the leaf traits. It is hence surprising that our reflectance measurements agree well with the values determined by Demarez for the forest at Fontainebleau, France, while leaf transmittances are partially different. This could be due to different versions of PROSPECT, where we used PROSPECT in its revision 5B (Feret et al., 2008) while Demarez probably used the original PROSPECT code (Jacquemoud and Baret, 1990).

Leaf reflectance varies only little between the top and the bottom of the canopy at Hohes Holz (Figure 4a-d) while leaf transmittance varies up to 0.1 between top and bottom of the canopy (Figure 4e-h). Leaves in the upper canopy receive more light, tend to be thicker and have higher leaf mass per area (LMA) than leaves lower down in the canopy (Demarez, 1999; Davi et al., 2008). LMA affects mostly leaf transmittance, which is consequently lower for thicker leaves. LMA affects less leaf reflectance, which depends in the visible spectrum more on leaf pigments (e.g. chlorophyll) and in the near infrared on dry matter and water content and leaf interior structure (Feret et al., 2008). Although variations of leaf transmittance were higher than of leaf reflectance, seasonal changes in the leaf phase function (here given as the ratio transmittance/albedo) were small between June and September for all species. Transmittance/albedo was lower at the top (≈0.45-0.5) and higher (≈ 0.5-.58) at the bottom due to higher leaf mass at the top of the canopy. We guess that effects of variations in leaf phase function on canopy transmittance are marginal compared to the effects which we considered, since variations in transmittance/albedo were small and since the effects of albedo on R^{NIR} were small.

However, replacing the observed and estimated NIR leaf reflectances and transmittances by the values from the literature in the FRT simulations decreased the mean leaf albedo by as little as 0.11 between May and September and decreased NIR canopy reflectance R^{NIR} by an average of 0.06 moving the simulation far away from the satellite observations (results not shown). We hence think that our estimates of leaf transmittance may be realistic for the forest Hohes Holz. In addition, the simulation with leaf properties from literature values showed the same seasonal decline of about 0.1 in R^{NIR} as the satellite observations and our *default* run. The strong decrease of R^{NIR} of 0.06 by changes in leaf albedo of 0.11 demonstrates the large sensitivity of canopy albedo to leaf optical properties. They do, however, only marginally influence the seasonal decline of NIR canopy reflectance R^{NIR} at the forest Hohes Holz.

4.6. Gap Fraction, LAI and Canopy Transmittance

Overstory LAI was nearly constant from mid May to end of September and had little effects on simulated NIR canopy reflectance (R^{NIR}, total effect $\delta_{t,5}$ = -0.01), gap fraction and canopy transmittance in our simulations. In general, variations of LAI have large effects on R^{NIR}, but the largest seasonal variations of overstory LAI, which happen during leaf unfolding in spring and leaf littering in autumn, were either before or after the investigated period at Hohes Holz in 2018. Additionally, during summer when LAI is highest the sensitivity of R^{NIR} towards changes of LAI $\left(\frac{\Delta R^{NIR}}{\Delta LAI}\right)$ was lowest in our simulations (Figure 11c). Similarly to R^{NIR}, the gap fraction in nadir direction saturated at LAI 2-3 in our simulations. This explained the time offset of about half a month between the onset of the decline of overstory LAI (second half of September) and the of increase of gap fraction and canopy transmittance (second half of October).

Although overstory LAI remained constant during the growing season, total LAI (i.e., the sum of overstory and understory LAI) may still have declined due to a decrease in understory LAI and contribute to a decline of R^{NIR} (Rautiainen et al., 2009). The seasonal course of total LAI at Hohes Holz in 2018 might have been similar to that by Rautiainen et al., since understory NIR reflectance decreased and R^{NIR} reflectance correlates well with LAI (e.g. *all constant except LAI* in Figure 9i or Jacquemoud (1993)). Another indicator for declining understory LAI was the decline of the understory greenness quantified by the green chromatic index (GCC) (Keenan et al. (2014), data not shown here).

Gap fraction at Hohes Holz seems to be a driver of R^{NIR} rather on the spatial scale than on the temporal scale. R^{NIR} was lower at locations with higher gap fraction (Figure 1) but gap fraction was stable during the main growing period (Figure 7b). We guess the reasons for decreasing R^{NIR} with increasing gap fraction are that first, soil absorbs more light than leaves in the NIR (c.f. Table 3) and second, the probability for light to escape the canopy is lower for light reflected by the soil, than for light reflected by leaves or woody material higher in the canopy.

4.7. Implications for GPP estimation from remote sensing

Several studies reported strong correlations between GPP and $\mathrm{NIR_V}$ or one of its modifications to account for radiation ($\mathrm{NIR_V} \cdot \mathrm{PAR}$ or $\mathrm{NIR_{V,\,rad}}$) in different ecosystems, also including forests (Badgley et al., 2017, 2019; Baldocchi et al., 2020; Dechant et al., 2020; Jiang et al., 2020; Wong et al., 2020; Wu et al., 2020). The results of Dechant et al. (2020) in crops suggest that the relationship between $\mathrm{NIR_V} \cdot \mathrm{PAR}$ and GPP goes beyond the light absorption component and is partly due to a correlation between the photosynthetic light use efficiency (LUE) and the escape fraction of NIR radiation from the canopy (f_{esc}).

Although the exact mechanism underlying the correlation between $\mathrm{NIR_V}$ and GPP is still unkown, canopy structure parameters such as LAI, leaf angles and clumping were identified as important factors (Badgley et al., 2019; Dechant et al., 2020; Zeng et al., 2019). In this study, we confirmed the importance of leaf angle changes for the seasonal dynamics of NIR reflectance, and hence, $\mathrm{NIR_V}$ (Figures 3, 9). However, we also identified two additional important factors that were not directly considered in previous literature on $\mathrm{NIR_V}$: the understory reflectance and the SZA.

Understory GPP reduction, e.g. via decreasing LAI, might be reflected in decreasing understory NIR reflectance. However, since forest GPP is typically dominated by the contribution of the overstory (Misson et al., 2007), the large understory effects on $\mathrm{NIR_V}$ (Figure 9) appear disproportionate compared to expected effects on GPP. This is further substantiated also by (Sampson et al., 2006), which found that understory contributed 10-20 % to overall GPP. Our findings may therefore indicate a weak link in the $\mathrm{NIR_V}$-GPP relationship at the level of the total canopy in ecoystems with complex, multi-layer canopies.

The statistical correlation between GPP and NIR_V with respect to SZA is just to some extent driven by a causal relationship. This mainly stems from corresponding irradiance changes. However, factors like temperature or water availability directly influence GPP and are largely independent of SZA. Incoming PAR is reduced with declining SZA towards autumn which proportionally reduces GPP but does effect NIR_V, but it directly affects the product $\mathrm{NIR_V} \cdot \mathrm{PAR}$ which was suggested to be a better proxy for GPP (Dechant et al., 2020). An indirect effect of solar angle on GPP might be mediated by leaf angles (see section 4.3), which affects both the fraction of absorbed PAR (fPAR) and the escape fraction, and hence $\mathrm{NIR_V}$. Such changes in leaf angles might go together with changes in biochemical leaf traits related to photosynthesis (Ollinger, 2011). Therefore, the decline in $\mathrm{NIR_V}$ (f_{esc}) may partly reflect physiological changes although via structural effects related to the solar angle and the leaf angles.

The global-scale findings of Badgley et al. (2019) suggest robust performance of $\mathrm{NIR_V}$ for forest GPP estimation at monthly time scales. Also, Wong et al. (2020) found that $\mathrm{NIR_V}$ captured the seasonal decline (summer-autumn) of GPP in a temperate mixed forest ecosystem rather well. As the links between $\mathrm{NIR_V}$ and GPP beyond light absorption are indirect and not due to strong mechanistic coupling, however, they might not hold in all situations or ecosystems. For example, Baldocchi et al. (2020) found evidence of lag effects between $\mathrm{NIR_{v,\,rad}}$ and GPP in corn and a wetland ecosystem. Our study identified potential weaknesses in the relationship between $\mathrm{NIR_V}$ and GPP in temperate broadleaf forests at seasonal time scales. To better understand the limitations of $\mathrm{NIR_V}$ as GPP proxy as well as identify potential mechanisms of covariation of leaf physiological and canopy structural traits (Ollinger, 2011), further detailed studies are needed.

5. Summary and Conclusions

We used both field observations and radiative transfer modelling to identify the main factors underlying the phenomenon of seasonally declining NIR reflectance in a temperate broadleaf forest. We found that understory reflectance had the largest effect on the simulations of NIR canopy reflectance $\mathrm{R^{NIR}}$, expressing the dynamic development of understory vegetation over the season and varying soil moisture levels. Leaf angles became more vertically oriented in summer compared to late spring throughout the whole canopy. This had the second strongest effect on $\mathrm{R^{NIR}}$. The solar zenith angle changes gradually over the seasons while the satellite's viewing angle varies but with no embedded trend. This sun-view geometry had the third largest effect on $\mathrm{R^{NIR}}$ in our simulations. The effect size does, however, depend on the viewing angle and might hence be different for other satellite missions or local instruments. Leaf optical properties did change only marginally throughout the season at Hohes Holz and leaf reflectance and transmittance had hence only minor effects on changes of $\mathrm{R^{NIR}}$. LAI variations were small between May and September and had the smallest effect on changes of $\mathrm{R^{NIR}}$ during that period.

Given our results, more extensive knowledge of seasonal changes of leaf angle distributions (LAD) is required, maybe facilitated by novel retrieval methods. LADs are assumed to be constant over the season in most land surface models. The influence of changing leaf angles should be assessed if these models are used to retrieve bio-physical parameters from satellite observations, for example. Most canopy radiative transfer schemes assume a nadir viewing angle of ingested satellite data. Our results indicate that even using maximal off-nadir Sentinel 2 a/b viewing angles (22.5°), observations still provide very similar results compared to nadir view. Our results also suggest that assuming constant leaf optical properties after the initial darkening of new leaves in spring might be sufficient to capture seasonal dynamics even when using the NIR waveband.

Our findings indicate a considerable complexity of the phenomenon of seasonally declining NIR reflectance as several different factors are involved. Apart from highlighting the need for more studies on seasonal understory and leaf angle dynamics, our study indicates potential weaknesses in the relationship between the NIR reflectance of vegetation canopies (NIRv) and GPP that should be investigated in more detail in the future.

Acknowledgments

We thank Gundula Schulz and Steffen Lehmann for massive help with the measurement campaign and the analsyis of leaf angle measurements, Andreas Schmidt and Maximilian Lange for helping to analyse the satellite observations and the in-situ spectral data, Andres Kuusk for help with the FRT model, Technicians from CHS for assistance with the measurements at Hohes Holz: Sebastian Gimper, Inmaculada Garcí Quirós, Laura Dienstbach, Patrick Schmidt, Marco Erfurth, Christian Wirth and Ronny Richter for providing arboretum access and Yasmin Möller for leaf cross cuts of the arboretum trees, Angel Naya Geiger and Nikolai Knapp for providing the canopy height plot (Hohes Holz) based on LIDAR measurements (Figure 1). Matthias Cuntz was supported by a grant overseen by the French National Research Agency (ANR) as part of the "Investissements d'Avenir" program (ANR-11-LABX-0002-01, Lab of Excellence ARBRE), by funding from ERA-NET Sumforest, funded by the European Union under Grant Agreement No. 606803 and in France through ANR (Grant No. ANR-16-SUMF-0001-01), and by a grant from the German Research Foundation (DFG, CU 173/4-1, PI 1179/2-1, WE 2681/10-1). We also thank four anonymous reviewers whose comments helped to improve the manuscript.

References

Badgley, G., Anderegg, L.D., Berry, J.A., Field, C.B., 2019. Terrestrial gross primary production: Using nirv to scale from site to globe. Global Change Biology URL: https://doi.org/10.1111/gcb.14729.

Badgley, G., Field, C.B., Berry, J.A., 2017. Canopy near-infrared reflectance and terrestrial photosynthesis. Science Advances 3, e1602244. doi:10.1126/sciadv.1602244.

Baldocchi, D.D., Ryu, Y., Dechant, B., Eichelmann, E., Hemes, K., Ma, S., Rey Sanchez, C., Shortt, R., Szutu, D., Valach, A., et al., 2020. Outgoing near infrared radiation from vegetation scales with canopy photosynthesis across a spectrum of function, structure, physiological capacity and weather. Journal of Geophysical Research: Biogeosciences , e2019JG005534doi:https://doi.org/10.1029/2019JG005534.

Blackburn, G., Milton, E., 1995. Seasonal variations in the spectral reflectance of deciduous tree canopies. International Journal of Remote Sensing 16, 709–720. URL: https://doi.org/10.1080/01431169508954435.

Bohn, F.J., Frank, K., Huth, A., 2014. Of climate and its resulting tree growth: Simulating the productivity of temperate forests. Ecological Modelling 278, 9–17. URL: https://doi.org/10.1016/j.ecolmodel.2014.01.021.

Bousquet, L., Lachérade, S., Jacquemoud, S., Moya, I., 2005. Leaf brdf measurements and model for specular and diffuse components differentiation. Remote Sensing of Environment 98, 201 – 211. URL: http://www.sciencedirect.com/science/article/pii/S0034425705002324, doi:https://doi.org/10.1016/j.rse.2005.07.005.

Butterfield, Z., Buermann, W., Keppel-Aleks, G., 2020. Satellite observations reveal seasonal redistribution of northern ecosystem productivity in response to interannual climate variability. Remote Sensing of Environment 242, 111755. URL: http://www.sciencedirect.com/science/article/pii/S0034425720301255, doi:https://doi.org/10.1016/j.rse.2020.111755.

Cailleret, M., Heurich, M., Bugmann, H., 2014. Reduction in browsing intensity may not compensate climate change effects on tree species composition in the bavarian forest national park. Forest ecology and management 328, 179–192.

Camps-Valls, G., Campos-Taberner, M., Moreno-Martinez, A., Walther, S., Duveiller, G., Cescatti, A., Mahecha, M.D., Munoz-Mari, J., Javier Garcia-Haro, F., Guanter, L., Jung, M., Gamon, J.A., Reichstein, M., Running, S.W., 2021. A unified vegetation index for quantifying the terrestrial biosphere. SCIENCE ADVANCES 7. doi:{10.1126/sciadv.abc7447}.

Croft, H., Chen, J., Froelich, N., Chen, B., Staebler, R., 2015. Seasonal controls of canopy chlorophyll content on forest carbon uptake: Implications for gpp modeling. Journal of Geophysical Research: Biogeosciences 120, 1576–1586. doi:https://doi.org/10.1002/2015JG002980.

Davi, H., Barbaroux, C., Dufrêne, E., Francois, C., Montpied, P., Bréda, N., Badeck, F., 2008. Modelling leaf mass per area in forest canopy as affected by prevailing radiation conditions. ecological modelling 211, 339–349.

Dechant, B., Cuntz, M., Vohland, M., Schulz, E., Doktor, D., 2017. Estimation of photosynthesis traits from leaf reflectance spectra: correlation to nitrogen content as the dominant mechanism. Remote Sensing of Environment 196, 279–292. URL: https://doi.org/10.1016/j.rse.2017.05.019.

Dechant, B., Ryu, Y., Badgley, G., Zeng, Y., Berry, J.A., Zhang, Y., Goulas, Y., Li, Z., Zhang, Q., Kang, M., et al., 2020. Canopy structure explains the relationship between photosynthesis and sun-induced chlorophyll fluorescence in crops. Remote Sensing of Environment 241, 111733.

Deering, D., Middleton, E., Eck, T., 1994. Reflectance anisotropy for a spruce-hemlock forest canopy. Remote Sensing of Environment 47, 242–260. URL: https://doi.org/10.1016/0034-4257(94)90159-7.

Deering, D.W., Eck, T.F., Grier, T., 1992. Shinnery oak bidirectional reflectance properties and canopy model inversion. IEEE Transactions on Geoscience and Remote Sensing 30, 339–348. doi:https://doi.org/10.1109/36.134083.

Demarez, V., 1999. Seasonal variation of leaf chlorophyll content of a temperate forest. inversion of the prospect model. International Journal of Remote Sensing 20, 879–894. doi:https://doi.org/10.1080/014311699212975.

Doxani, G., Vermote, E., Roger, J.C., Gascon, F., Adriaensen, S., Frantz, D., Hagolle, O., Hollstein, A., Kirches, G., Li, F., et al., 2018. Atmospheric correction inter-comparison exercise. Remote Sensing 10, 352.

Eriksson, H.M., Eklundh, L., Kuusk, A., Nilson, T., 2006. Impact of understory vegetation on forest canopy reflectance and remotely sensed lai estimates. Remote Sensing of Environment 103, 408–418. doi:https://doi.org/10.1016/j.rse.2006.04.005.

Feret, J.B., François, C., Asner, G.P., Gitelson, A.A., Martin, R.E., Bidel, L.P., Ustin, S.L., le Maire, G., Jacquemoud, S., 2008. Prospect-4 and 5: Advances in the leaf optical properties model separating photosynthetic pigments. Remote Sensing of Environment 112, 3030 – 3043. URL: http://www.sciencedirect.com/science/article/pii/S0034425708000813, doi:http://dx.doi.org/10.1016/j.rse.2008.02.012.

Fisher, J.I., Mustard, J.F., Vadeboncoeur, M.A., 2006. Green leaf phenology at landsat resolution: Scaling from the field to the satellite. Remote Sensing of Environment 100, 265 – 279. URL: http://www.sciencedirect.com/science/article/pii/S0034425705003597, doi:https://doi.org/10.1016/j.rse.2005.10.022.

Gielen, B., Acosta, M., Altimir, N., Buchmann, N., Cescatti, A., Ceschia, E., Fleck, S., Hortnagal, L., Klumpp, K., Kolari, P., et al., 2018. Ancillary vegetation measurements at icos ecosystem stations .

Grant, L., 1987. Diffuse and specular characteristics of leaf reflectance. Remote Sensing of Environment 22, 309 – 322. URL: `http://www.sciencedirect.com/science/article/pii/0034425787900642`, doi:`https://doi.org/10.1016/0034-4257(87)90064-2`.

Hapke, B., DiMucci, D., Nelson, R., Smythe, W., 1996. The cause of the hot spot in vegetation canopies and soils: Shadow-hiding versus coherent backscatter. Remote Sensing of Environment 58, 63–68. doi:`https://doi.org/10.1016/0034-4257(95)00257-X`.

Häusler, M., Silva, J.M., Cerasoli, S., López-Saldaña, G., Pereira, J.M., 2016. Modelling spectral reflectance of open cork oak woodland: a simulation analysis of the effects of vegetation structure and background. International Journal of Remote Sensing 37, 492–515. doi:`https://doi.org/10.1080/01431161.2015.1134847`.

Holtmann, A., Huth, A., Pohl, F., Rebmann, C., Fischer, R., 2021. Carbon Sequestration in Mixed Deciduous Forests: The Influence of Tree Size and Species Composition Derived from Model Experiments. FORESTS 12. doi:`{10.3390/f12060726}`.

Hovi, A., Raitio, P., Rautiainen, M., et al., 2017. A spectral analysis of 25 boreal tree species. Silva Fennica 51. doi:`https://doi.org/10.14214/sf.7753`.

Huete, A.R., 1987. Soil and sun angle interactions on partial canopy spectra. International Journal of Remote Sensing 8, 1307–1317. doi:`https://doi.org/10.1080/01431168708954776`.

Jacquemoud, S., 1993. Inversion of the prospect + sail canopy reflectance model from aviris equivalent spectra: Theoretical study. Remote Sensing of Environment 44, 281 – 292. URL: `http://www.sciencedirect.com/science/article/pii/003442579390022P`, doi:`https://doi.org/10.1016/0034-4257(93)90022-P`.

Jacquemoud, S., Baret, F., 1990. Prospect: A model of leaf optical properties spectra. Remote Sensing of Environment 34, 75–91.

Jiang, C., Guan, K., Wu, G., Peng, B., Wang, S., 2020. A daily, 250 m, and real-time gross primary productivity product (2000–present) covering the contiguous united states. Earth System Science Data Discussions , 1–28.

Jiao, T., Liu, R., Liu, Y., Pisek, J., Chen, J.M., 2014. Mapping global seasonal forest background reflectivity with multi-angle imaging spectroradiometer data. Journal of Geophysical Research: Biogeosciences 119, 1063–1077. doi:`https://doi.org/10.1002/2013JG002493`.

Keenan, T., Darby, B., Felts, E., Sonnentag, O., Friedl, M., Hufkens, K., O'Keefe, J., Klosterman, S., Munger, J.W., Toomey, M., et al., 2014. Tracking forest phenology and seasonal physiology using digital repeat photography: a critical assessment. Ecological Applications 24, 1478–1489. doi:`https://doi.org/10.1890/13-0652.1`.

Kimes, D.S., Newcomb, W.W., Nelson, R.F., Schutt, J.B., 1986. Directional reflectance distributions of a hardwood and pine forest canopy. IEEE Transactions on Geoscience and Remote Sensing , 281–293doi:`https://doi.org/10.1109/TGRS.1986.289647`.

King, D.A., 1997. The functional significance of leaf angle in eucalyptus. Australian Journal of Botany 45, 619–639. doi:`https://doi.org/10.1071/BT96063`.

Kolle, O., Rebmann, C., 2007. Eddysoft - Documentation of a Software Package to Acquire and Process Eddy Covariance Data. Technical Report 10. Max-Planck-Institute for Biogeochemistry. Jena, Germany.

Kuusk, A., 1995. A fast, invertible canopy reflectance model. Remote Sensing of Environment 51, 342–350.

Kuusk, A., 2001. A two-layer canopy reflectance model. Journal of Quantitative Spectroscopy and Radiative Transfer 71, 1–9.

Kuusk, A., Kuusk, J., Lang, M., 2014. Modeling directional forest reflectance with the hybrid type forest reflectance model frt. Remote Sensing of Environment 149, 196 – 204. URL: `http://www.sciencedirect.com/science/article/pii/S0034425714001370`, doi:`https://doi.org/10.1016/j.rse.2014.03.035`.

Kuusk, A., Nilson, T., 2000. A directional multispectral forest reflectance model. Remote Sensing of Environment 72, 244–252.

Lang, A., Xiang, Y., 1986. Estimation of leaf area index from transmission of direct sunlight in discontinuous canopies. Agricultural and Forest Meteorology 37, 229–243.

Lange, M., Dechant, B., Rebmann, C., Vohland, M., Cuntz, M., Doktor, D., 2017. Validating modis and sentinel-2 ndvi products at a temperate deciduous forest site using two independent ground-based sensors. Sensors 17, 1855.

Liu, J., Skidmore, A.K., Wang, T., Zhu, X., Premier, J., Heurich, M., Beudert, B., Jones, S., 2019. Variation of leaf angle distribution quantified by terrestrial lidar in natural european beech forest. ISPRS journal of photogrammetry and remote sensing 148, 208–220.

Liu, Y., Wu, C., Sonnentag, O., Desai, A.R., Wang, J., 2020. Using the red chromatic coordinate to characterize the phenology of forest canopy photosynthesis. Agricultural and Forest Meteorology 285, 107910.

Louis, J., Debaecker, V., Pflug, B., Main-Knorn, M., Bieniarz, J., Mueller-Wilm, U., Cadau, E., Gascon, F., 2016. Sentinel-2 sen2cor: L2a processor for users, in: Proceedings Living Planet Symposium 2016, Spacebooks Online. pp. 1–8.

Ma, X., Huete, A., Tran, N.N., 2019. Interaction of seasonal sun-angle and savanna phenology observed and modelled using modis. Remote Sensing 11, 1398.

Majasalmi, T., Rautiainen, M., 2020. The impact of tree canopy structure on understory variation in a boreal forest. Forest Ecology and Management 466, 118100.

McNeil, B.E., Pisek, J., Lepisk, H., Flamenco, E.A., 2016. Measuring leaf angle distribution in broadleaf canopies using uavs. Agricultural and Forest Meteorology 218, 204–208.

Middleton, E.M., 1991. Solar zenith angle effects on vegetation indices in tallgrass prairie. Remote Sensing of Environment 38, 45–62.

Misson, L., Baldocchi, D., Black, T., Blanken, P., Brunet, Y., Yuste, J.C., Dorsey, J., Falk, M., Granier, A., Irvine, M., et al., 2007. Partitioning forest carbon fluxes with overstory and understory eddy-covariance measurements: A synthesis based on fluxnet data. Agricultural and Forest Meteorology 144, 14–31.

Mollenhauer, H., Pflug, B., Lausch, A., Borg, E., Mollenhauer, O., Dietrich, P., Bumberger, J., 2017. Mobile wireless sensor networks for ground truthing multispectral remotely sensed data .

Mõttus, M., Sulev, M., Hallik, L., 2014. Seasonal course of the spectral properties of alder and birch leaves. IEEE Journal of Selected Topics in Applied Earth Observations and Remote Sensing 7, 2496–2505.

Mullen, K., Ardia, D., Gil, D.L., Windover, D., Cline, J., 2011. Deoptim: An r package for global optimization by differential evolution. Journal of Statistical Software 40, 1–26.

Nagai, S., Nasahara, K.N., Muraoka, H., Akiyama, T., Tsuchida, S., 2010a. Field experiments to test the use of the normalized-difference vegetation index for phenology detection. Agricultural and Forest Meteorology 150, 152–160.

Nagai, S., Saigusa, N., Muraoka, H., Nasahara, K.N., 2010b. What makes the satellite-based evi–gpp relationship unclear in a deciduous broad-leaved forest? Ecological Research 25, 359–365.

Nagler, P., Daughtry, C., Goward, S., 2000. Plant litter and soil reflectance. Remote Sensing of Environment 71, 207–215.

Niinemets, Ü., 2010. A review of light interception in plant stands from leaf to canopy in different plant functional types and in species with varying shade tolerance. Ecological Research 25, 693–714.

Nikopensius, M., Pisek, J., Raabe, K., 2015. Spectral reflectance patterns and seasonal dynamics of common understory types in three mature hemi-boreal forests. International Journal of Applied Earth Observation and Geoinformation 43, 84–91.

Ollinger, S., 2011. Sources of variability in canopy reflectance and the convergent properties of plants. New Phytologist 189, 375–394.

Piayda, A., Dubbert, M., Werner, C., Correia, A.V., Pereira, J.S., Cuntz, M., 2015. Influence of woody tissue and leaf clumping on vertically resolved leaf area index and angular gap probability estimates. Forest Ecology and Management 340, 103–113.

Pisek, J., 2018. 3.07 - forest background, in: Liang, S. (Ed.), Comprehensive Remote Sensing. Elsevier, Oxford, pp. 78 – 103. URL: `https://www.sciencedirect.com/science/article/pii/B9780124095489105238`, doi:`https://doi.org/10.1016/B978-0-12-409548-9.10523-8`.

Pisek, J., Chen, J.M., Kobayashi, H., Rautiainen, M., Schaepman, M.E., Karnieli, A., Sprinstin, M., Ryu, Y., Nikopensius, M., Raabe, K., 2016. Retrieval of seasonal dynamics of forest understory reflectance from semiarid to boreal forests using modis brdf data. Journal of Geophysical Research: Biogeosciences 121, 855–863.

Pisek, J., Erb, A., Korhonen, L., Biermann, T., Carrara, A., Cremonese, E., Cuntz, M., Fares, S., Gerosa, G., Grünwald, T., Hase, N., Heliasz, M., Ibrom, A., Knohl, A., Kobler, J., Kruijt, B., Lange, H., Leppänen, L., Limousin, J.M., Serrano, F.R.L., Loustau, D., Lukeš, P., Lundin, L., Marzuoli, R., Mölder, M., Montagnani, L., Neirynck, J., Peichl, M., Rebmann, C., Rubio, E., Santos-Reis, M., Schaaf, C., Schmidt, M., Simioni, G., Soudani, K., Vincke, C., 2021. Retrieval and validation of forest background reflectivity from daily moderate resolution imaging spectroradiometer (modis) bidirectional reflectance distribution function (brdf) data across european forests. Biogeosciences 18, 621–635. URL: `https://bg.copernicus.org/articles/18/621/2021/`, doi:`10.5194/bg-18-621-2021`.

Pisek, J., Sonnentag, O., Richardson, A.D., Mõttus, M., 2013. Is the spherical leaf inclination angle distribution a valid assumption for temperate and boreal broadleaf tree species? Agricultural and Forest Meteorology 169, 186–194.

R Core Team, 2018. R: A Language and Environment for Statistical Computing. R Foundation for Statistical Computing. Vienna, Austria. URL: `https://www.R-project.org/`.

Raabe, K., Pisek, J., Sonnentag, O., Annuk, K., 2015. Variations of leaf inclination angle distribution with height over the growing season and light exposure for eight broadleaf tree species. Agricultural and forest meteorology 214, 2–11. URL: `https://www.sciencedirect.com/science/article/pii/S0168192315002154`.

Rautiainen, M., Lang, M., Mõttus, M., Kuusk, A., Nilson, T., Kuusk, J., Lükk, T., 2008. Multi-angular reflectance properties of a hemiboreal forest: An analysis using chris proba data. Remote Sensing of Environment 112, 2627–2642.

Rautiainen, M., Mõttus, M., Heiskanen, J., Akujärvi, A., Majasalmi, T., Stenberg, P., 2011. Seasonal reflectance dynamics of common understory types in a northern european boreal forest. Remote Sensing of Environment 115, 3020–3028.

Rautiainen, M., Nilson, T., Lükk, T., 2009. Seasonal reflectance trends of hemiboreal birch forests. Remote Sensing of Environment 113, 805–815.

Reaves, V., Elmore, A., Nelson, D., McNeil, B., 2018. Drivers of spatial variability in greendown within an oak-hickory forest landscape. Remote Sensing of Environment 210, 422–433.

Ridler, T., Calvard, S., et al., 1978. Picture thresholding using an iterative selection method. IEEE trans syst Man Cybern 8, 630–632.

Ross, J., 1981. The radiation regime and architecture of plant stands. Springer Science & Business Media.

Roy, D.P., Li, J., Zhang, H.K., Yan, L., Huang, H., Li, Z., 2017. Examination of sentinel-2a multi-spectral instrument (msi) reflectance anisotropy and the suitability of a general method to normalize msi reflectance to nadir brdf adjusted reflectance. Remote Sensing of Environment 199, 25–38.

Ryu, Y., Sonnentag, O., Nilson, T., Vargas, R., Kobayashi, H., Wenk, R., Baldocchi, D.D., 2010. How to quantify tree leaf area index in an open savanna ecosystem: a multi-instrument and multi-model approach. Agricultural and Forest Meteorology 150, 63–76.

Saltelli, A., Ratto, M., Andres, T., Campolongo, F., Cariboni, J., Gatelli, D., Saisana, M., Tarantola, S., 2008. Global sensitivity analysis: the primer. John Wiley & Sons.

Sampson, D.A., Janssens, I.A., Ceulemans, R., 2006. Under-story contributions to stand level GPP using the process model SECRETS. AGRICULTURAL AND FOREST METEOROLOGY 139, 94–104. doi:{10.1016/j.agrformet.2006.06.003}.

Schneider, C.A., Rasband, W.S., Eliceiri, K.W., 2012. NIH Image to ImageJ: 25 years of image analysis. Nature methods 9, 671.

Suviste, S., Nilson, T., Lukk, T., Eenmae, A., 2007. Seasonal reflectance course of some forest types in estonia from multi-year landsat tm and spot images and via simulation, in: Analysis of Multi-temporal Remote Sensing Images, 2007. MultiTemp 2007. International Workshop on the, IEEE. pp. 1–5.

Syren, P., 1994. Reflectance anisotropy for nadir observations of coniferous forest canopies. Remote Sensing of Environment 49, 72–80.

Thimonier, A., Sedivy, I., Schleppi, P., 2010. Estimating leaf area index in different types of mature forest stands in switzerland: a comparison of methods. European Journal of Forest Research 129, 543–562.

Vermote, E.F., Tanré, D., Deuze, J.L., Herman, M., Morcette, J.J., 1997. Second simulation of the satellite signal in the solar spectrum, 6s: An overview. IEEE transactions on geoscience and remote sensing 35, 675–686.

Vicari, M.B., Pisek, J., Disney, M., 2019. New estimates of leaf angle distribution from terrestrial lidar: Comparison with measured and modelled estimates from nine broadleaf tree species. Agricultural and forest meteorology 264, 322–333.

Wang, Q., Adiku, S., Tenhunen, J., Granier, A., 2005. On the relationship of ndvi with leaf area index in a deciduous forest site. Remote Sensing of Environment 94, 244–255.

Widlowski, J.L., Mio, C., Disney, M., Adams, J., Andredakis, I., Atzberger, C., Brennan, J., Busetto, L., Chelle, M., Ceccherini, G., et al., 2015. The fourth phase of the radiative transfer model intercomparison (rami) exercise: Actual canopy scenarios and conformity testing. Remote Sensing of Environment 169, 418–437.

Wilson, J.W., 1960. Inclined point quadrats. New Phytologist 59, 1–7.

Wong, C.Y., D'Odorico, P., Arain, M.A., Ensminger, I., 2020. Tracking the phenology of photosynthesis using carotenoid-sensitive and near-infrared reflectance vegetation indices in a temperate evergreen and mixed deciduous forest. New Phytologist 226, 1682–1695. URL: https://nph.onlinelibrary.wiley.com/doi/abs/10.1111/nph.16479, doi:10.1111/nph.16479, arXiv:https://nph.onlinelibrary.wiley.com/doi/pdf/10.1111/nph.16479.

Wu, G., Guan, K., Jiang, C., Peng, B., Kimm, H., Chen, M., Yang, X., Wang, S., Suyker, A.E., Bernacchi, C.J., et al., 2020. Radiance-based nirv as a proxy for gpp of corn and soybean. Environmental Research Letters 15, 034009.

Wutzler, T., Lucas-Moffat, A., Migliavacca, M., Knauer, J., Sickel, K., Sigut, L., Menzer, O., Reichstein, M., 2018. Basic and extensible post-processing of eddy covariance flux data with REddyProc. BIOGEOSCIENCES 15, 5015–5030. doi:{10.5194/bg-15-5015-2018}.

Yang, X., Tang, J., Mustard, J.F., 2014. Beyond leaf color: Comparing camera-based phenological metrics with leaf biochemical, biophysical, and spectral properties throughout the growing season of a temperate deciduous forest. Journal of Geophysical Research: Biogeosciences 119, 181–191.

Yang, X., Tang, J., Mustard, J.F., Wu, J., Zhao, K., Serbin, S., Lee, J.E., 2016. Seasonal variability of multiple leaf traits captured by leaf spectroscopy at two temperate deciduous forests. Remote Sensing of Environment 179, 1–12.

Zeng, Y., Badgley, G., Dechant, B., Ryu, Y., Chen, M., Berry, J.A., 2019. A practical approach for estimating the escape ratio of near-infrared solar-induced chlorophyll fluorescence .

Zhang, X., Friedl, M.A., Schaaf, C.B., Strahler, A.H., 2004. Climate controls on vegetation phenological patterns in northern mid-and high latitudes inferred from modis data. Global Change Biology 10, 1133–1145.